Title
Assessment of ozone photochemistry in the western North Pacific as inferred from PEM-West A observations during the fall 1991

Journal
Journal of Geophysical Research Atmospheres, 101(D1)

ISSN
0148-0227

Authors
Davis, DD
Crawford, J
Chen, G
et al.

Publication Date
1996

DOI
10.1029/95JD02755

JOURNAL OF GEOPHYSICAL RESEARCH, VOL. 101, NO. D1, PAGES 2111-2134, JANUARY 20, 1996

Assessment of ozone photochemistry in the western North Pacific as inferred from PEM-West A observations during the fall 1991

D. D. Davis,[1] J. Crawford,[1] G. Chen,[1] W. Chameides,[1] S. Liu,[2] J. Bradshaw,[1] S. Sandholm,[1] G. Sachse,[3] G. Gregory,[3] B. Anderson,[3] J. Barrick,[3] A. Bachmeier,[3] J. Collins,[3] E. Browell,[3] D. Blake,[4] S. Rowland,[4] Y. Kondo,[5] H. Singh,[6] R. Talbot,[7] B. Heikes,[8] J. Merrill,[8] J. Rodriguez,[9] and R. E. Newell[10]

Abstract. This study examines the influence of photochemical processes on ozone distributions in the western North Pacific. The analysis is based on data generated during NASA's western Pacific Exploratory Mission (PEM-West A) during the fall of 1991. Ozone trends were best described in terms of two geographical domains: the western North Pacific rim (WNPR) and the western tropical North Pacific (WTNP). For both geographical regions, ozone photochemical destruction, $D(O_3)$, decreased more rapidly with altitude than did photochemical formation, $F(O_3)$. Thus the ozone tendency, $P(O_3)$, was typically found to be negative for $z < 6$ km and positive for $z > 6$-8 km. For nearly all altitudes and latitudes, observed nonmethane hydrocarbon (NMHC) levels were shown to be of minor importance as ozone precursor species. Air parcel types producing the largest positive values of $P(O_3)$ included fresh continental boundary layer (BL) air and high-altitude ($z > 7$ km) parcels influenced by deep convection/lightning. Significant negative $P(O_3)$ values were found when encountering clean marine BL air or relatively clean lower free-tropospheric air. Photochemical destruction and formation fluxes for the Pacific rim region were found to exceed average values cited for marine dry deposition and stratospheric injection in the northern hemisphere by nearly a factor of 6. This region was also found to be in near balance with respect to column-integrated O_3 photochemical production and destruction. By contrast, for the tropical regime column-integrated O_3 showed photochemical destruction exceeding production by nearly 80%. Both transport of O_3 rich midlatitude air into the tropics as well as very high-altitude (10-17 km) photochemical O_3 production were proposed as possible additional sources that might explain this estimated deficit. Results from this study further suggest that during the fall time period, deep convection over Asia and Malaysia/Indonesia provided a significant source of high-altitude NO_x to the western Pacific. Given that the high-altitude NO_x lifetime is estimated at between 3 and 9 days, one would predict that this source added significantly to high altitude photochemical O_3 formation over large areas of the western Pacific. When viewed in terms of strong seasonal westerly flow, its influence would potentially span a large part of the Pacific.

[1]School of Earth and Atmospheric Sciences, Georgia Institute of Technology, Atlanta.
[2]Environmental Research Labs, NOAA Aeronomy Laboratory, Boulder, Colorado.
[3]NASA Langley Research Center, Hampton, Virginia
[4]Chemistry Department, University of California-Irvine.
[5]Solar Terrestrial Environmental Laboratory, Nagoya University, Toyokawa, Aichi, Japan.
[6]NASA Ames Research Center, Moffett Field, California
[7]Institute for the Study of Earth, Oceans, and Space, University of New Hampshire, Durham.
[8]Graduate School of Oceanography, University of Rhode Island, Narragansett.
[9]AER Incorporated, Cambridge, Massachusetts.
[10]Massachusetts Institute of Technology, Department of Earth, Atmosphere and Planetary Sciences, Cambridge.

Paper number 95JD02755.
0148-0227/96/95JD-02755$05.00

Introduction

Since the early 1970s when the first papers appeared raising the issue of photochemical production of ozone in the remote troposphere [*Chameides and Walker*, 1973; *Crutzen*, 1973]; the topic of tropospheric sources and sinks of ozone has been one of intense scientific investigation and debate [e.g., *Fabian*, 1974; *Chameides and Walker*, 1973; *Chatfield and Harrison*, 1976; *Fabian and Pruchniewicz*, 1977; *Fishman et al.*, 1979; *Liu et al.*, 1980; *Gidel and Shapiro*, 1980; *Mahlman et al.*, 1980; *Chameides and Tan*, 1981; *Logan et al.*, 1981]. The preponderance of evidence now suggests that both transport and photochemical factors play an important role in controlling the tropospheric distribution of ozone (see previous list of references). Of the two factors, however, the contribution from photochemical processes is generally viewed as having the larger uncertainty. This partially reflects the fact that the photochemical

models from which global photochemical rates have been assessed are based on globally "estimated" distributions of the critical precursor species such as NO, CO, H_2O, and non-methane hydrocarbons (NMHCs) [cf. *Fishman and Crutzen*, 1978; *Liu et al.*, 1980; *Chameides and Tan*, 1981; *Logan et al.*, 1981]. In fact, significant uncertainties still remain in these "estimated" distributions. This is particularly true as related to NO, NMHCs, and H_2O (e.g., upper free troposphere).

From a mechanistic point of view, there also remain significant questions concerning some gas phase chemical processes (i.e. halogen chemistry) as well as physical removal processes and heterogeneous chemical reactions. Thus both mechanistic deficiencies as well as the absence of comprehensive O_3 precursor databases suggest that our assessment of tropospheric ozone as driven by photochemical processes is still in need of intensive study.

The focus of this study will be on assessing the influence of photochemical processes on ozone distributions in the western North Pacific. The database used in this analysis was that generated during the NASA Pacific Exploratory Mission in the western Pacific (PEM-West A) in the fall of 1991 [see *Hoell et al.*, this issue]. Because of the large geographical scope of this airborne field study, it has provided an excellent opportunity to compare photochemical modeling results from real-time observations with those based on more generic global databases.

Specific objectives of this study include (1) investigating the relative importance of ozone-controlling factors such as NO_x, NMHCs, H_2O, and peroxy radical levels; (2) assessing the trends in photochemical ozone formation and destruction as a function of altitude and geographical location; (3) examining the relationship between air mass types and the magnitude/sign of the ozone tendency; (4) investigating potential sources of NO_x; and (5) examining the tropospheric ozone budget in the western North Pacific.

Observational Database

Measurements

A detailed listing of all PEM-West A airborne measurements has been provided by *Hoell et al.* [this issue]. Also reported for each instrument are the data sampling rate, precision, accuracy, and nominal limit of detection (LOD). The data sampling rate during PEM-West A varied from a high of one measurement every 5 s (i.e., CO, CH_4, CO_2, and N_2O) to a low of one sample every 15 to 40 min (i.e., HNO_3). The fastest time resolution used in this analysis was 3 min. This resolution allowed for an extensive analysis of photochemical O_3 formation, $F(O_3)$, destruction, $D(O_3)$, and tendency, $P(O_3)$, as well as meaningful comparisons between predicted and observed values of several photochemical test species such as NO_2, H_2O_2, and CH_3OOH (see discussion below under "Model Description").

The only adjustment to the database as reported in the final data archive involved the "discontinuous" NMHC data reported by *Blake et al.*, [this issue]. In this case a survey of the PEM-West A database revealed that of 1085 data points with acceptable NO, CO, O_3, and H_2O measurements only 631 of these had corresponding NMHC data. Of the 454 runs without NMHC data, 313 of these were assigned values based on interpolation. The criteria for interpolation involved there being present bracketing NMHC values that were within a factor of 1.3 of each other as well as significant continuity in the mixing ratios for the variables CO and O_3. For the 141 remaining cases, NMHC mixing ratios were assigned based on median values for each hydrocarbon species. These median values were defined in terms of the entire PEM-West A data set as subdivided into 1-km altitude bins and as further subdivided into two different latitude ranges, i.e., 0°-18°N and 18°-42°N.

For the critical parameters NO and H_2O, two independent databases were recorded. Each was based on an independent measurement technique. For NO the techniques were two-photon laser-induced fluorescence (TPLIF) provided by Georgia Institute of Technology (GIT), and O_3-chemiluminescence (CHEMI-L) provided by Nagoya University (NU) [*Kondo et al.*, this issue]. An analysis of these independent data sets showed quite good agreement, e.g., typically within 30%. Reflecting this level of agreement, the procedure adopted in using these two data sets followed one of six scenarios: (1) when only CHEMI-L data were available, the observed values were used without modification. (2) When only TPLIF data were reported, again these values were used without modification. (3) When only limit of detection values were reported, an NO value was assigned equal to the investigator's cited LOD. (4) When values were reported by both techniques and either reported an NO level of less than 20 parts per trillion by volume (pptv), a simple arithmetic average of the two values was taken. (5) When values were reported by both techniques and both values were greater than 20 pptv but were within a factor of 2.0 of each other, again a simple arithmetic average of the two values was taken. (6) When values were reported for both techniques in which both were greater than 20 pptv but differed by greater than a factor of 2.0, the TPLIF value was taken. Quite noteworthy here is the fact that the latter scenario occurred less than 1% of the time when both techniques reported data.

Concerning H_2O measurements, both a GE1011 frost point hygrometer and a Lyman α fluorescence sensor were used to record H_2O levels during PEM-West A. The Lyman α sensor, having been designed for very low water environments, was not operated below 5.5 km. Thus all dew point measurements reported at altitudes below 5.5 km were those recorded with the frost point hygrometer. For very dry atmospheric conditions, e.g., air parcels having dew point depressions of greater than 45° at static air temperatures of 0°C, the Lyman α sensor was taken as the more reliable reading. In the special case where cloud conditions were encountered, the value assigned for the dew point was the same as that for the static air temperature.

In several cases our analyses have required the use of either NO_2 and/or NO_y data. For NO_2 we have used only model-calculated values. (See discussion under "Model Description" for further details.) These calculated values have been labeled in the text as $(NO_2)_{mc}$; similarly, values for NO_x (i.e., the summation of $(NO)_{meas}+(NO_2)_{mc}$) have been labeled $(NO_x)_{mc}$. For NO_y, two independent data sets were reported involving two different instruments; however, in this case significant disagreement was found between the two sets of observations. Both instruments used a gold surface in the presence of added CO gas to catalytically convert NO_y to NO, but each system had its own unique sample inlet and detection method for NO. In our analysis we have elected to use only the GIT data. This decision was

based on the recommendation made by a "Blue Ribbon evaluation panel" [*Crosley*, this issue].

Geographical Distribution and Concentration Levels

Figure 1a shows the geographical distribution of data recorded during PEM-West A that have been used in the current analysis. It encompasses 1085 independent observations in the western Pacific, all of which were recorded during flights 6-18. Additional data (i.e., 140 data points) were recorded during transit flights between San Francisco, California and Anchorage, Alaska; Anchorage, Alaska and Yokota, Japan; Wake Island and Hawaii; and Hawaii and San Francisco. These data were viewed as more representative of the central and eastern North Pacific and therefore will be treated as part of a future study.

Figure 1b shows the same data set as presented in Figure 1a but plotted as a function of latitude and altitude. We note that only those observations having solar zenith angles of $<70°$ are shown since only these data were used in our analysis. With the possible exception of one altitude block in the tropics (i.e., 10-12 km), Figure 1b illustrates that a reasonable distribution of data was available covering most altitudes over the latitude range of 0°-42°N.

An assessment of these data with regard to latitude and trace gas concentration levels is shown in Figures 2a and 2b. In this case for illustration purposes we show plotted the two critical photochemical species, NO and O_3. (Still other concentration/latitude plots may be found in *Blake et al.* [this issue] and *Kondo et al.* [this issue]). For both NO and O_3 it can be seen that a significant gradient in mixing ratios occurs over the latitude range of 16°-22°N, with 18°N defining the sharpest transition. This point is further illustrated in the form of Table 1 where the mean, standard deviation, median, and max and min values for several photochemical species are presented for the latitudinal breakouts of 0°-18°N and 18°-42°N. From these summary data it is apparent that mixing ratios for all five species (i.e., NO, O_3, CO, C_3H_8, C_6H_6) have significantly greater variability and larger mean and median values for the high-latitude regime. In particular, O_3, NO, and the NMHCs have median values which differ by nearly factors of 2 for these two regimes. Reflecting these gradients in O_3 and NO, Figure 2c shows that model-calculated values of the photochemical ozone tendency also display a strong latitudinal dependence.

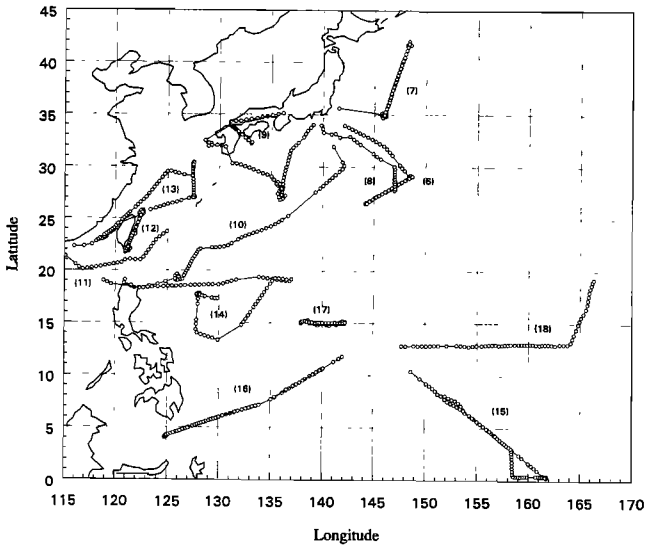

Figure 1a. PEM-West A data collection region. Flight numbers are indicated in parentheses. Symbols indicate location of in situ measurements used in photostationary state (PSS) model calculations.

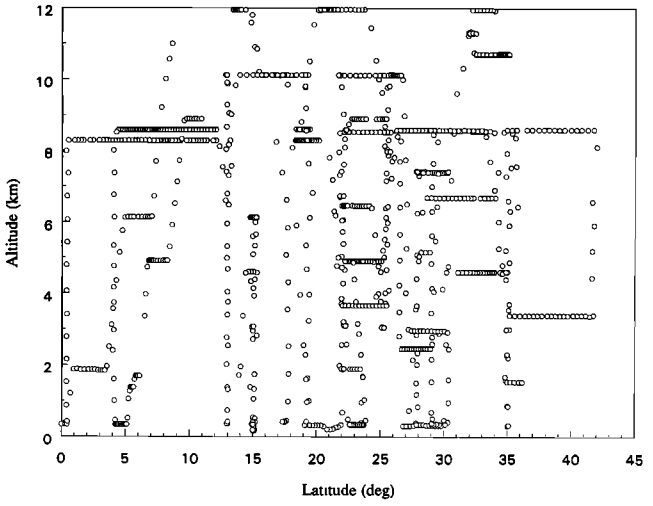

Figure 1b. Latitude and altitude distribution of in situ measurements used in PSS model calculations.

In addition to the gradients observed as a function of latitude, significant shifts in trace gas mixing ratios were also seen as a function of altitude. For most species, however, this trend was much weaker than that observed with latitude. It also tended to be quite nonuniform. For some species, low-altitude values exceeded those at high-altitudes; for others the trend was reversed, and in still other cases mid-altitude values were lower than either those at high or low-altitudes [e.g., *Blake et al.* this issue; *Kondo et al.*, this issue]. Of the species listed in Table 1, NO was unique in having a strong positive vertical gradient. As shown in Figure 3, a rather dramatic upward ramping in the NO mixing ratio is seen, with the most abrupt change occurring at altitudes near 6 or 7 km. Although this trend was characteristic of both the high and the low-latitude regimes, it was far more pronounced at high-latitudes. For the entire data set (neglecting 15 data points near the coasts of Japan and China), the median NO mixing ratio is estimated to change by nearly a factor of 6 over the altitude range of 0 to 12 km.

As illustrated in Figure 2c, differences in the distribution of ozone precursor species with latitude and altitude had a significant impact on the calculated photochemical formation, destruction, and tendency of O_3. For this reason, much of the analysis that follows will focus on comparing and contrasting the photochemical environments of two regions. The western North Pacific rim (coordinates: 135° to 150°E at 42°N and 112° to 148°E at 18°N, labeled hereinafter WNPR) may be characterized as a region influenced by both natural and anthropogenic continental sources. In particular, available evidence points toward this region as having been significantly impacted by high-altitude (e.g., 6-12 km) outflow from the Asian continent and quite likely from other

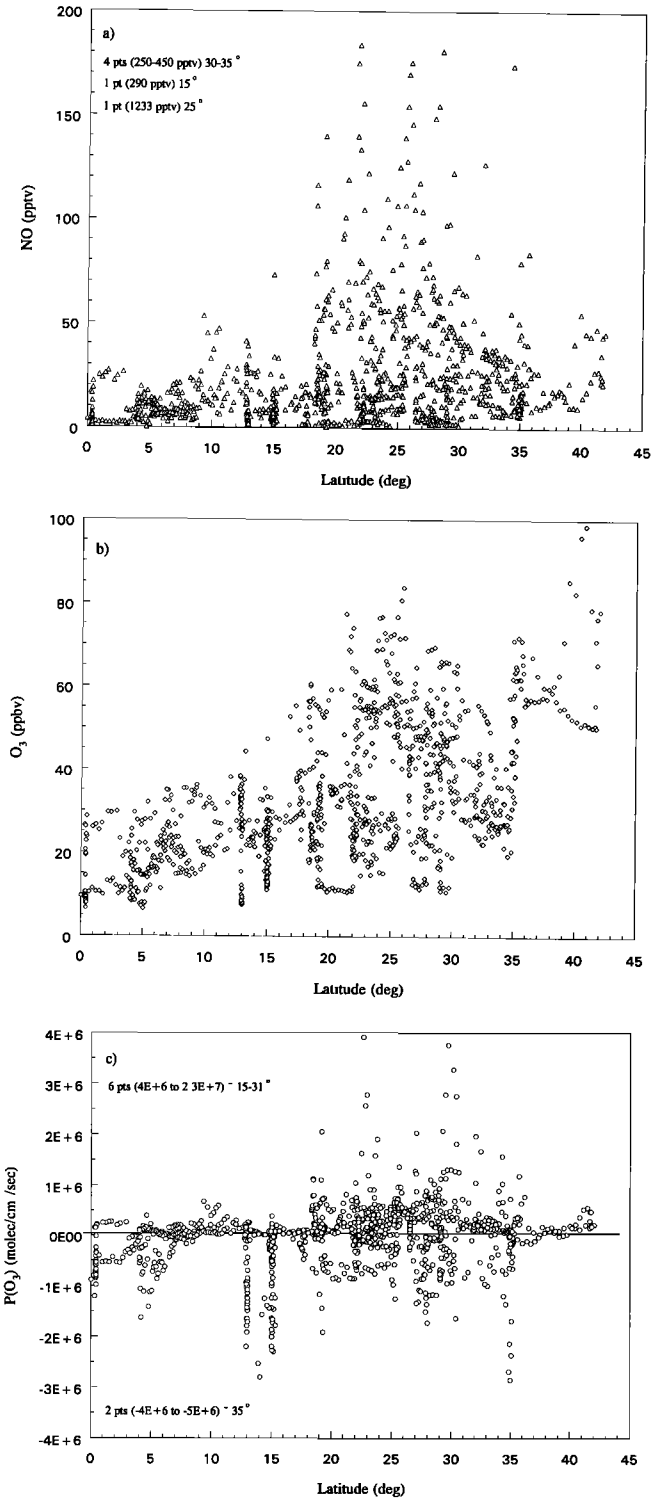

Figure 2. Scatterplots showing the latitude distribution of (a) NO, (b) O_3, and (c) $P(O_3)$.

northern hemispheric continents. By contrast, the western tropical North Pacific at altitudes <10 km (coordinates: 127° to 167°E at 18°N and 124° to 168°E at 0°, labeled hereinafter WTNP) can be viewed as a region whose chemical fingerprint reflected either aged/well-processed continental air or air masses that had their origin in the tropical/equatorial Pacific. (see also discussions by *Liu et al.* [this issue], *Smyth et al.* [this issue], *Talbot et al.* [this issue], *Gregory et al.*[this issue], and *Browell et al.* [this issue].

Data Analysis

Photochemistry

The photochemistry of O_3 within the troposphere is initiated by the UV photolysis of O_3 at wavelengths <315 nm

(R1) $O_3 + h\nu \rightarrow O_2 + O(^1D)$

Most of the time the highly reactive photofragment, $O(^1D)$, is collisionally deactivated (e.g., M = N_2 and/or O_2)

(R2) $O(^1D) + M \rightarrow O(^3P) + M^*$

to form ground state atomic oxygen, thus leading to the rapid reformation of O_3 via (R3)

(R3) $O(^3P) + O_2 + M \rightarrow O_3 + M$

A very small fraction of the $O(^1D)$, however, reacts with gas phase H_2O to generate the centrally important oxidizing species OH

(R4) $O(^1D) + H_2O \rightarrow 2OH$

Reaction (R4) therefore is important because it both represents a primary source of tropospheric OH radicals and serves as a sink for O_3. The OH species itself can undergo still further reaction, leading to the formation of O_3. For example, OH readily reacts with CO, CH_4, as well as with most NMHCs to produce the peroxy radical species HO_2, CH_3O_2, and RO_2 (R = C_2H_5 and higher organic groupings). If adequate levels of NO are available, peroxy radicals react to form NO_2 via (R5), (R6), and (R7)

(R5) $HO_2 + NO \rightarrow OH + NO_2$

(R6) $CH_3O_2 + NO \rightarrow CH_3O + NO_2$

Table 1. Observations of NO, O_3, CO, and C_3H_8 for Sampling Zones, 0°-18° N and 18°-42° N

0°-18° N	Mean[a]	s.d.	Median[a]	Max[a]	Min[a]
NO, pptv	11.5	17.0	8.2	293	1.5[b]
O_3, ppbv	21.7	8.9	22	55	7
CO, ppbv	88.6	17.3	86	149	67
C_3H_8, pptv	40.1	44.8	30	285	6.5
C_6H_6, pptv	22.2	18.4	18	126	5[c]
18°-42° N	**Mean[a]**	**s.d.**	**Median[a]**	**Max[a]**	**Min[a]**
NO, pptv	34.6	60.1	21.3	1233	1.5[b]
O_3, ppbv	39.9	16.6	38	99	11
CO,ppbv	98.1	20.3	96	186	66
C_3H_8,pptv	89.2	129.9	59	1362	7
C_6H_6, pptv	37.7	35.1	28	268	5[c]

[a]Includes all data modelled (i.e. 0-70 degrees solar zenith angle)
[b]Denotes a limit of detection for TPLIF NO measurements
[c]Denotes a limit of detection measurement

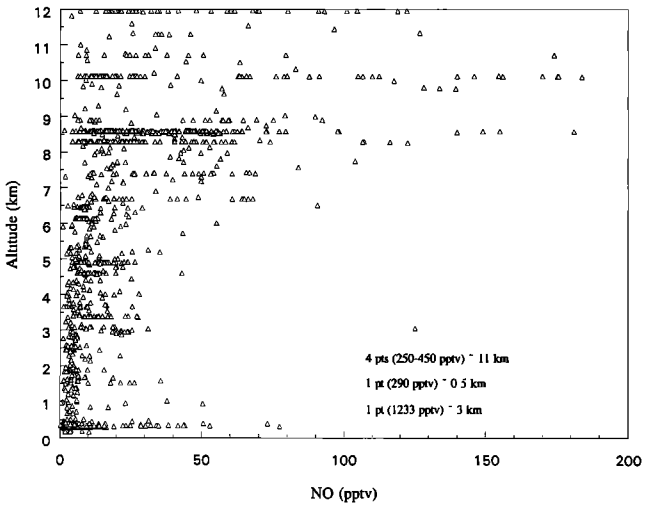

Figure 3. Scatterplot showing the altitude distribution of NO.

(R7) $RO_2 + NO \rightarrow RO + NO_2$

The NO_2 species is then rapidly photolyzed in the troposphere to form $O(^3P)$ and NO which, via reaction (R3), leads to the formation of a new O_3 molecule. But since more than one peroxy radical can be generated for each primary OH (see, for example, reaction (R5)), several O_3 molecules can potentially be produced each time reaction (R4) occurs.

For atmospheric regions which are NO poor, the peroxy radical self-reaction (R8) increases in importance,

(R8) $HO_2 + HO_2 \rightarrow H_2O_2 + O_2$

as well as reaction with O_3,

(R9) $HO_2 + O_3 \rightarrow OH + 2O_2$

If the latter reaction takes place, it also represents a photochemical loss of O_3. An additional minor sink for O_3 involves its reaction with OH,

(R10) $OH + O_3 \rightarrow HO_2 + O_2$

Based on processes (R1)-(R10), the rate-limiting reactions controlling ozone can be expressed in terms of the difference between O_3 formation and destruction, e.g., O_3 photochemical tendency, $P(O_3)$. Accordingly, $P(O_3)$ can be represented by equation (1):

$$P(O_3) = \{k_5[HO_2] + k_6[CH_3O_2] + k_7[RO_2]\}[NO] - \{k_4[O(^1D)][H_2O] + k_9[HO_2][O_3] + k_{10}[OH][O_3]\} \quad (1)$$

where the brackets indicate the concentration of each species and the individual "k_i" terms represent the appropriate gas kinetic rate constant for each reaction. From an inspection of equation (1), it is apparent that the value of $P(O_3)$ can be either positive or negative. When $P(O_3)$ is >0, photochemical processes provide a net source of O_3 to the troposphere; when <0, they provide a net sink. Thus the numerical value of $P(O_3)$ is a convenient way to estimate the net effect of photochemistry on ambient levels of O_3.

For purposes of comparing photochemical fluxes with other O_3 source and sink fluxes, the quantities $F(O_3)$, the photochemical formation rate,

$$F(O_3) = \{k_5[HO_2] + k_6[CH_3O_2] + k_7[RO_2]\}[NO] \quad (2)$$

and $D(O_3)$, the photochemical destruction rate,

$$D(O_3) = k_4[O(^1D)][H_2O] + k_9[HO_2][O_3] + k_{10}[OH][O_3] \quad (3)$$

will also prove to be useful.

Still more speculative in nature have been suggestions by some investigators that halogen species might play a significant role in controlling tropospheric levels of O_3 [*Chameides and Davis,* 1980; *Singh and Kasting*, 1988; *Barrie et al.*, 1988; *Bottenheim et al.*, 1990; *Chatfield and Crutzen,* 1990; *Keene et al.*, 1990; *Jenkin*, 1993; *Jobson et al.*, 1994; *Le Bras and Platt,* 1995; *Solomon et al.*, 1995; *Singh et al.*, this issue; and *Davis et al.*, this issue]. Key processes here involve the reaction sequence (R11)-(R14):

(R11) $X + O_3 \rightarrow XO + O_2$

(R12) $XO + XO \rightarrow 2X + O_2$

(R13) $XO + HO_2 \rightarrow HOX + O_2$

(R14) $HOX + h\nu \rightarrow OH + X$

Thus either through (R11) and (R12) or, alternatively, (R11), (R13), and (R14), halogen chemistry can lead to the net destruction of ozone. *Davis et al.*, [this issue] have recently reviewed the tropospheric chemistry of halogens with respect to their potential impact on O_3. For tropical and midlatitudes these authors have concluded that for the halogens bromine and chlorine the most likely impact would be found in the marine BL. However, even in this environment, evaluation of the source strengths for the reactive forms of these halogens was viewed as being highly speculative in that heterogeneous sources had to be invoked. By comparison, the evaluations for iodine were far more quantitative since the major source for reactive iodine involved the gas phase photolysis of iodocarbons. A summary of these results has been presented below in the text under the "Discussion" section.

Model Description

Two types of box models were used in this study: instantaneous photostationary state (PSS) and time-dependent (TD). Both have been previously described by *Chameides et al.* [1987, 1989] and *Davis et al.* [1993]. Changes to these earlier models, as reflected in this study, have been addressed in a companion paper by *Crawford et al.* [this issue]. Summarized below are the salient features of these two models.

In the instantaneous photostationary state model, all photochemical species are assumed to be in photochemical equilibrium. The use of this model in this study was for purposes of evaluating photochemical products for individual data points. Even so, it is important to recognize that the actual spatial scale encompassed by each data point was typically quite large. It is defined by the product of the aircraft speed and the time resolution employed for the input

data to the model. As noted earlier, the time resolution selected for this analysis was 3 min. Hence, each independent modeling result, reflecting one input data point, is the average result over a sampling range of nearly 37 km.

Input to the PSS model consisted of fixed values for the mixing ratios of the chemical observables O_3, NO, H_2O, CO, NMHC and the physical parameters temperature, pressure, and UV solar flux. For H_2 and CH_4, global average mixing ratios were taken, e.g., 0.55 and 1.7 parts per million by volume(ppmv), respectively. As noted above, the concentrations of the short-lived species HO_2, OH, $O(^1D)$, CH_3O, CH_3O_2, RO_2, NO_2, and NO_3 as well as the chemically related species CH_2O, HO_2NO_2, and N_2O_5 were evaluated by setting the rate of production for each species equal to the rate of destruction. Intermediate-lived species such as HNO_3, H_2O_2, and CH_3OOH were also assumed to reach steady state (at high-altitudes this list would also include N_2O_5 and HO_2NO_2). For each of the latter species, in addition to the known gas phase reactions, a heterogeneous loss was assumed that was similar to that described by *Logan et al.* [1981]. This computational format has been labeled here as our "unconstrained" or "standard" model run. A second PSS format, involving the use of measured concentrations for the species NO_2, H_2O_2, CH_3OOH, HNO_3 and peroxy-acetyl nitrate (PAN) has been labeled "constrained"; and still a third PSS model version, involving NMHC levels being set equal to zero, is labeled here "No NMHC."

Time-dependent box model runs were used to generate diurnal profiles for both radical species and the modeling products $F(O_3)$, $D(O_3)$, and $P(O_3)$. These runs were also used to evaluate quasi steady state levels of HNO_3 and NO_x based on the photochemical recycling of NO_y. For this study, Time Dependent Model (TDM) values have been reported for 14 different chemical environments (data bins) as defined by seven altitude ranges and two latitudinal regimes. Input data for these runs consisted of median values for CO, H_2O, O_3, NMHCs, T, and P. Typically, between 10 and 140 data points were available to define these median values.

A critical piece of input to the TDM was the NO mixing ratio. For this study this quantity was established by invoking a constant daytime only NO source flux. This flux was then adjusted so as to give back an NO value corresponding to the median level estimated for a specific altitude/latitude bin. Daytime NO median levels were estimated using data that were filtered for solar zenith angles of 0° to 60°. For internal consistency, all other input data used in our TDM runs were also filtered with a 0° to 60° zenith angle restriction. Depending on ambient conditions, TDM runs typically required 20 to 100 days to reach a quasi steady state solution.

A detailed comparison of our PSS model-estimated levels of OH and HO_2 with those of *J. Rodriguez et al.* (private communication, 1995) showed the agreement to be within ±13% (for details see *Crawford et al.* [this issue].) Further consistency checks of the current PSS model with experimental observations involved comparisons for NO_2, H_2O_2, and CH_3OOH. The results are shown in Figures 4a-4c.

We note that for the species H_2O_2 and CH_3OOH, only free-tropospheric altitudes were considered due to the enhanced uncertainty associated with cloud washout, precipitation removal, and surface deposition at BL altitudes.

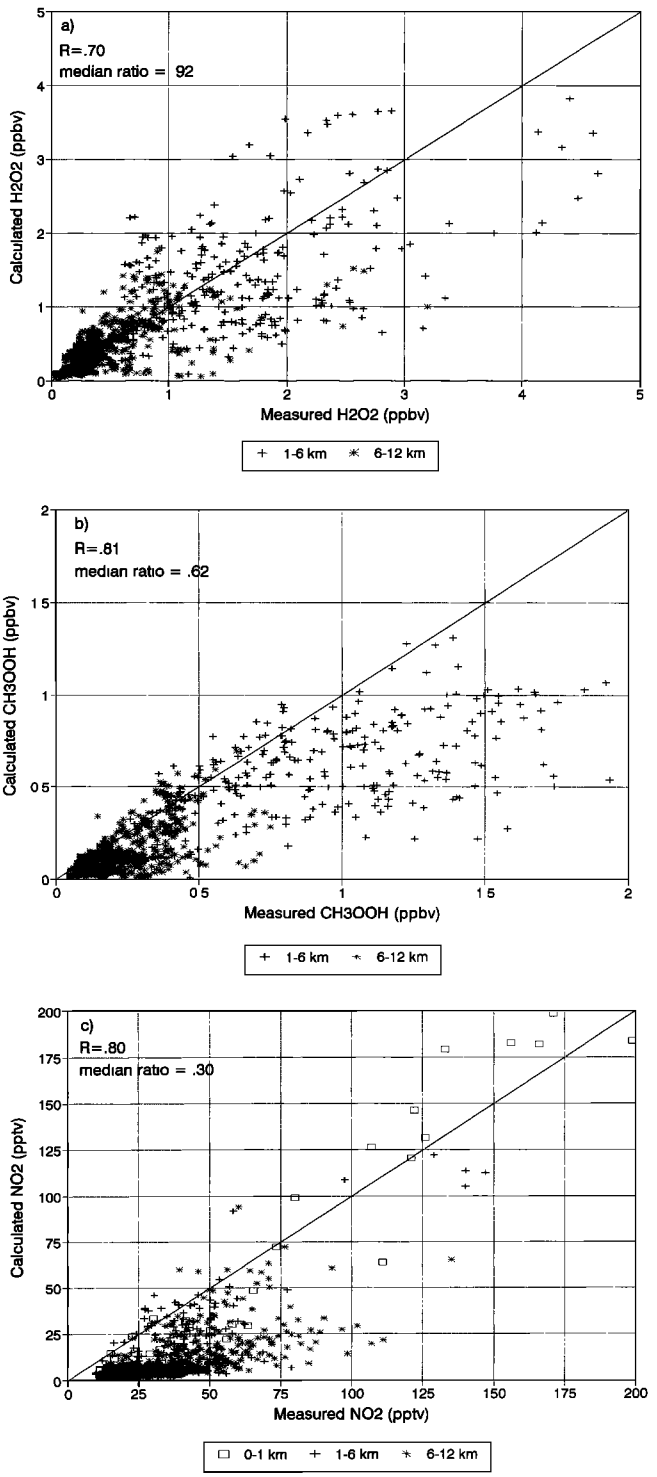

Figure 4. Scatterplots comparing measured and PSS model-calculated values of (a) H_2O_2, (b) CH_3OOH, and (c) NO_2. Unity line is provided for reference purposes.

When comparing H_2O_2 levels at free-tropospheric altitudes, the agreement between model predictions and observations is seen as quite good. For example, the median value for the ratio $(H_2O_2)_{mc}/(H_2O_2)_{expt}$ is 0.92, and the Pearson "r" correlation coefficient is estimated at 0.74. For CH_3OOH the agreement is not quite so good, the model-calculated values being nearly a factor of 1.6 lower than those ob-

served; however, the "r" value is still found to be quite significant, i.e., 0.81. Equally important, the level of disagreement lies well within the combined uncertainties (e.g., factor of 2.5) of two of the critical rate coefficients that control the CH_3OOH species, i.e. $HO_2 + CH_3O_2$ and $CH_3OOH + OH$. Other possible sources of systematic error could include (1) the accuracy of the CH_3OOH measurements themselves or (2) the combined uncertainty associated with the experimental input data to the model. (For further details on the comparison of model and observed levels of peroxide species, the reader is referred to *Heikes et al.* [this issue].

By far the poorest level of agreement is seen in the comparison of the model-predicted and measured values of NO_2. For example, from Figure 4c, the median value of $(NO_2)_{mc}/(NO_2)_{expt}$ is estimated as 0.3. At present we believe this disagreement is suggestive of an NO_2 measurement interference, although possible shortcomings in the model chemistry cannot be totally ruled out. (For a far more exhaustive discussion of all aspects of the comparison between NO_2 observations and model predictions the reader is referred to *Crawford et al.* [this issue].)

Ozone Photochemical Trends: Flight Track Analysis

As discussed earlier in the text, during PEM-West A, significant chemical differences were found between observations recorded in the tropics versus those recorded at higher latitudes in what has been labeled the "western North Pacific rim" region. As illustrative of some of these differences, Figures 5a-5c show time series plots for two flights in the Pacific rim region (flights 10 and 12) and one in the tropics (flight 15). In particular, these flights attempt to provide further insight concerning the levels and sources of NO_x which have a major impact on the evaluated photochemical O_3 trends. To aid in this discussion, we have plotted five key parameters: altitude, solar zenith angle, NO, CO, and C_3H_8 together with the O_3 modeling products $D(O_3)$, $F(O_3)$, and $P(O_3)$.

Flight 10. Flight 10 was designated a "survey" flight since all profiling took place while the aircraft was in transit from Yokota, Japan to Okinawa. For this Pacific rim flight the 10-day isentropic back trajectories [*Merrill*, this issue] indicate that for altitudes <6 km the origin of the air mass sampled was the central Pacific. The trajectories also suggest that this air had no recent contact with a land mass. As shown in Figure 5a, this "background" air description seems to be reflected quite nicely in the observed low to modest levels of all three tracer species NO, CO, and C_3H_8.

At high-altitudes ($z > 6$ km) and still early in the flight (3.25 to 4.5 GMT) the trajectories also indicate a marine origin; but these air parcels are then shown as moving close to Taiwan and the Asian mainland before moving northwestward and being intercepted by the DC-8 aircraft. Later in the flight (7.25 to 9.25 GMT), while still at high-altitudes, the back trajectories appear to originate just to the south of Taiwan. This air mass is then seen moving very slowly eastward before being intercepted near Okinawa. For both sampling periods, however, evidence exists that suggests that the chemical composition of the air sampled was influenced by deep convection over land. For example, Figure 5a shows significant enhancements in NO, CO, and C_3H_8, all with a reasonably high level of correlation based on a simple

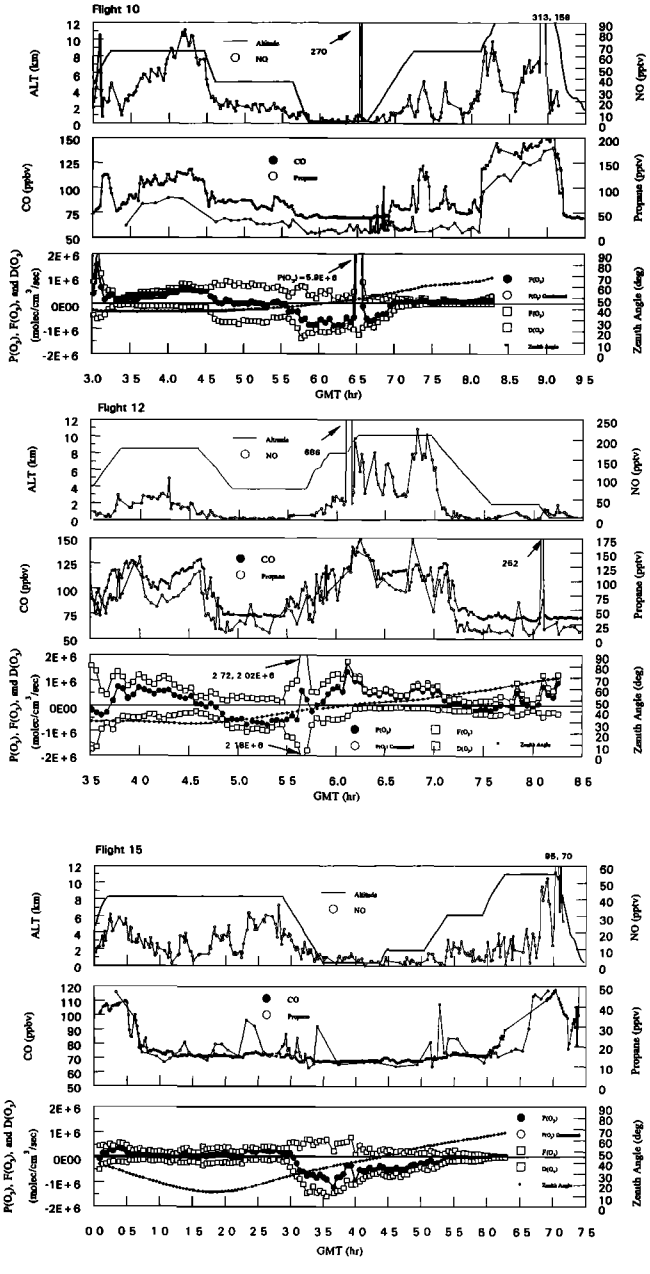

Figure 5. Time series plots from flights 10, 12, and 15. Top panel shows variations in altitude and measured NO. Middle panel shows variations in CO and C_3H_8. The bottom panel shows variations in solar zenith angle and $F(O_3)$, $D(O_3)$, and $P(O_3)$ as calculated from PSS model runs. Constrained and unconstrained $P(O_3)$ results are distinguishable only if constrained values deviate from unconstrained by more than 15%.

visual inspection. In fact, during the 12-km leg, the levels of NO, CO, and C_3H_8 are shown reaching values of 313 pptv, 150 ppbv, and 175 pptv, respectively. Quite interestingly, the 313 pptv of NO was recorded under dusk solar conditions. In addition, during the final 3 hours of the flight, approximately 150 lightning signatures were recorded with an onboard storm scope. This instrument has an estimated range of 300 km. Satellite imagery also indicated that the general region of sampling was influenced by severe tropical

storm Nat. This storm was located between Hong Kong and southern Taiwan during the flight, and the satellite images showed a well-organized area of convection had formed just to the east of Taiwan.

As seen in Figure 5a, for daylight conditions the highest values for both $F(O_3)$ and $D(O_3)$ occur at altitudes <6 km. At BL altitudes, where levels of NO were <10 pptv, this is observed to result in significant net O_3 destruction, e.g., -6 to -9×10^5 molecules/cm^3/s. At higher altitudes, where the NO mixing ratio is seen approaching 90 pptv, $P(O_3)$ values are observed as high as $+6\times10^5$ molecules/cm^3/s and remain generally positive over the entire leg during daylight hours.

Flight 12. Flight 12 originated out of Hong Kong and was designed to look at high-altitude outflow from the Asian continent. The sampling profile was a standard "wall" profile (for detailed description see *Hoell et al.* [this issue]), and was configured geographically to be approximately 30 km to the east of the island of Taiwan. The setting for flight 12 was quite different from flight 10 in that the high-altitude ($z>6$-km) air trajectories indicate that the air mass sampled was less than one day removed from the Asian mainland. On the other hand, the <6-km trajectories generally show a picture not that different from flight 10, namely, that the air mass sampled was marine in origin. As shown in Figure 5b, this assessment is in reasonable agreement with the chemical observations in that low to moderate levels are seen for all three tracer species.

At higher altitudes the chemical composition is seen as being far more variable. Like flight 10, the mixing ratios for all three tracers are found to be significantly greater at high-altitudes. For example, during the 10-km sampling run, the mixing ratios for NO, CO, and C_3H_8 are seen reaching 225 pptv, 175 ppbv, and 175 pptv, respectively. For NO and C_3H_8 these values are 5 times greater than those observed at low-altitude. Although the correlation between the individual tracers is qualitatively not so high as in flight 10, it is still quite significant.

Satellite imagery showed that tropical storm Nat continued to move slowly northeastward and thus had a significant influence on the outflow sampled during flight 12. Embedded thunderstorms were evident along significant stretches of the east China coast. In fact, quite similar to flight 10 approximately 100 lightning signatures were recorded during flight 12. Collectively, the available evidence suggests that during flight 12 the outflow from mainland China was strongly influenced by deep convection. It also appears that this deep convection had a major impact on the concentration profiles of the tracer species NO, CO, and C_3H_8.

From Figure 5b it can be seen that for both high and low-altitudes, $F(O_3)$ and $D(O_3)$ display a wide range of values. Reflecting the elevated levels of NO observed at high-altitude, $P(O_3)$ values are seen as being predominantly positive, with some values ranging up to $+1\times10^6$ molecules/cm^3/s. For altitudes <6 km, involving background marine air, $P(O_3)$ ranges between zero and -1×10^6 molecules/cm^3/s. The very low-altitude positive values of $P(O_3)$, observed for GMT times of 7.25 and higher, reflect low-altitude pollution from the southern tip of Taiwan. These observations were made on the return trip to Hong Kong.

Flight 15. Flight 15 is representative of the WTNP sampling regime in that O_3 and its photochemical precursor species were typically quite low. This flight was staged out of Guam and involved an "extended wall profile." The flight was designed to sample as far south as the equator following a southeast vector out from Guam. The 10-day back trajectories suggest that at all altitudes the air mass sampled originated over the ocean and had no significant interaction with any landmass. At altitudes <6 km the chemical data appears to support this picture of a clean marine environment. Typical levels of NO, CO, and C_3H_8 are seen from Figure 5c to be 10 pptv, 70 ppbv, and 15 pptv, respectively. However, at altitudes >8 km the chemical tracer data suggest otherwise. For the 8.2 and 11 km data runs, Figure 5c shows that for three different time periods enhanced levels of NO appear. These are seen to be qualitatively correlated with elevated levels of propane and in two cases with elevated levels of CO. Like flights 10 and 12, high-altitude levels of NO and C_3H_8 are seen exceeding those at low-altitude by factors in excess of 3. For CO the high-altitude enhancement was closer to a factor of 1.5. As was the case in flight 10, during the high-altitude sampling run at 11 km, the 95 pptv NO peak was recorded under dusk conditions.

Satellite imagery showed that cirrus outflow from Typhoon Pat, located to the north, had reached the general vicinity of Guam. In addition, scattered areas of deep convection could be identified to the southeast of Guam. Although no storm scope data were available for flight 15, the chemical and satellite data again seem to suggest that deep convection was a major factor in defining the air composition at high-altitudes. Since marine BL levels of NO, CO, and C_3H_8 were typically observed to be quite low, it also suggests that this convection occurred either over an island or some other major landmass. Similarly, some high-altitude segments of tropical flights 14 and 16 also showed trace gas distributions which were consistent with deep convection over a landmass of some type.

The O_3 photochemical profile for flight 15 is one that strongly reflects variations in the NO_x environment. For example, under daylight conditions, Figure 5c shows that at low-altitudes ($z<5$ km) the NO mixing ratio was typically <10 pptv; as a result the net effect of photochemistry on O_3 is one that shows net destruction. Like flights 10 and 12 therefore the low-altitude $P(O_3)$ values for flight 15 are seen to range down to -1×10^6 molecules/cm^3/s. And even at high-altitudes, because of low average values for NO, $P(O_3)$ values remain low, e.g., zero or slightly positive. Positive values occur when the NO mixing ratio exceeds 15-20 pptv. This situation is seen for GMT times 0.2 to 0.75 and 2.25 to 3.0. During these time periods $P(O_3)$ is observed reaching a value of $+3\times10^5$ molecules/cm^3/s. Given more favorable solar conditions, the time period 6.75 to 7.25 would also have yielded very positive values of $P(O_3)$ as is also true for the previously discussed 12 km sampling run during flight 10. (For still additional information on individual flight track analyses and the use of chemical tracers to identify NO_x sources, the reader is referred to *D. Davis et al.* [manuscript in preparation, 1995] and *Kondo et al.* [this issue]).

Ozone Photochemical Trends: Latitude and Altitude

Because both $D(O_3)$ and $F(O_3)$ have a strong functional dependence on solar zenith angle, a quantitative comparison of the PSS results requires a more selective solar filter than that imposed on the initial data set, e.g., 0°-70°. Thus for

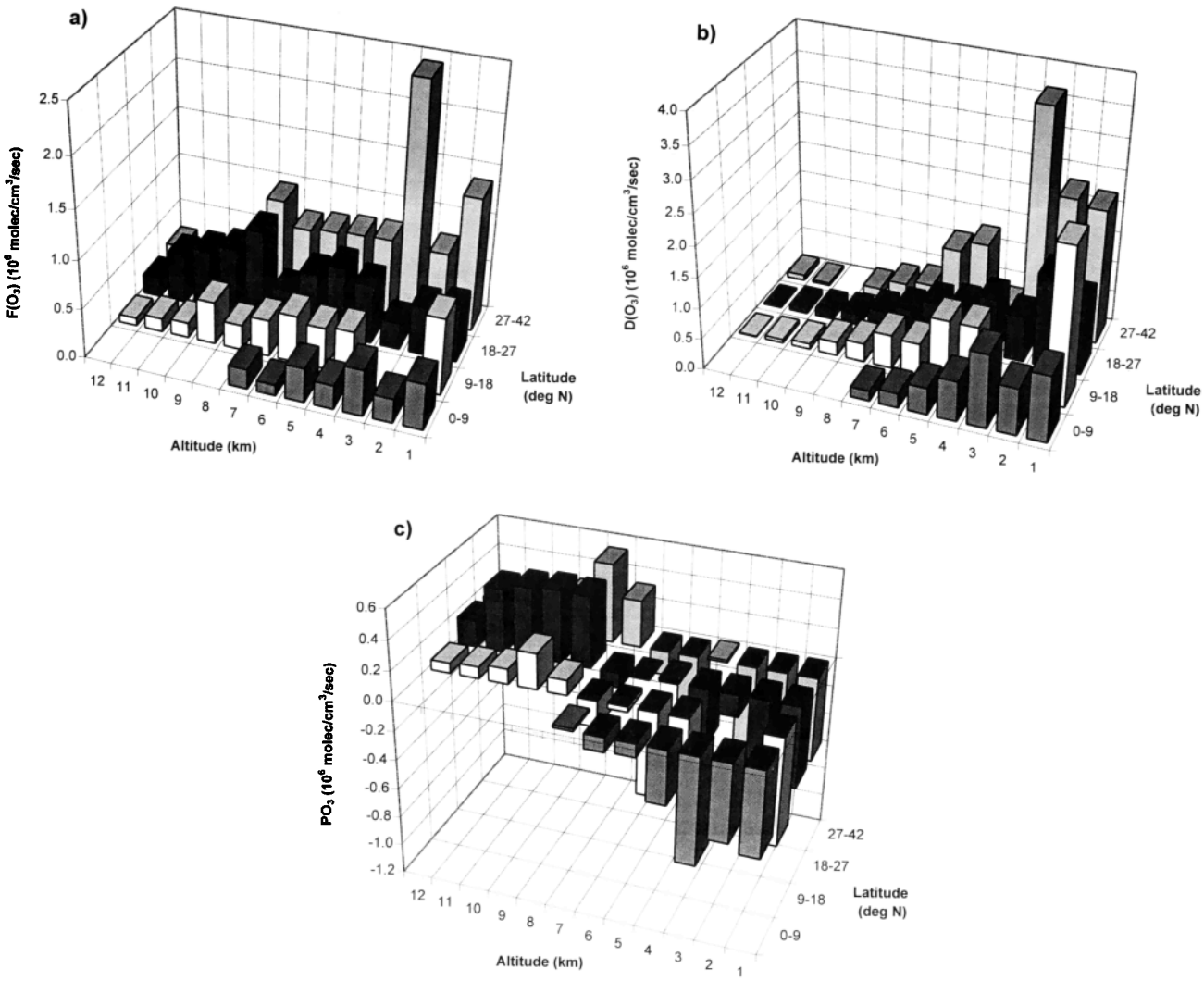

Figure 6. Latitude and altitude distributions of (a) $F(O_3)$, (b) $D(O_3)$, and (c) $P(O_3)$. Values given for each bin represent median values estimated from PSS model runs. Only data recorded for solar zenith angles of 30° to 60° are shown. Bins without values contained less than three data points.

purposes of this data analysis we have further filtered our original data runs so as to include only zenith angles between 30° and 60°. The net effect of this filtering has been to reduce the total number of usable data points from 1085 to 760. However, under this more restricted Z-angle range, the corresponding range for the calculated parameters $D(O_3)$ and $F(O_3)$ (for similar chemical conditions) has been reduced to factors of 1.5 to 2.0. This filtered data set is shown here in Figures 6a-6c. In this case the data have been "binned" according to altitude and latitude dimensions of 1 km and 9°, respectively. In these plots, only bins having three or more data points are shown; and of those bins assigned values, 70% had nine or more data points. Even so, it is important to keep in mind that the data collection period that formed the basis for Figures 6a-6c, as well as the subsequent three dimensional plots, 7a-7h, represent but a chemical snap shot of the western Pacific. In some cases these plots also average away very modest longitudinal gradients. Thus the representativeness of these plots must be viewed with some element of caution.

From an analysis of Figure 6c, two general trends in $P(O_3)$ emerge: (1) at altitudes below 6 km, values are consistently negative with the larger of these occurring within the first 3 to 4 km of the surface. (2) Above 7 km $P(O_3)$ values tend to be positive, but the magnitude is found to be strongly dependent on latitude. For example, values in the WNPR region tend to be 2 to 4 times higher than those in the tropics (see also Tables 2a and 2b).

Figures 6a and 6b show the variability in $D(O_3)$ and $F(O_3)$ as a function of altitude and latitude. Quite clearly, the trends in these two calculated quantities are significantly different. $D(O_3)$ values drop precipitously with increasing altitude at all latitudes. By contrast, values of $F(O_3)$ are seen to fluctuate by factors of 2 to 3, but no systematic trend is observed over the full range of altitude, i.e., 0 to 12 km. In addition, the values of $F(O_3)$ in the WNPR region tend to be significantly higher than those for the tropical regime.

Collectively, these results show that the observed increase in positive values of $P(O_3)$ with increasing altitude can be understood in terms of large decreases in the value of $D(O_3)$

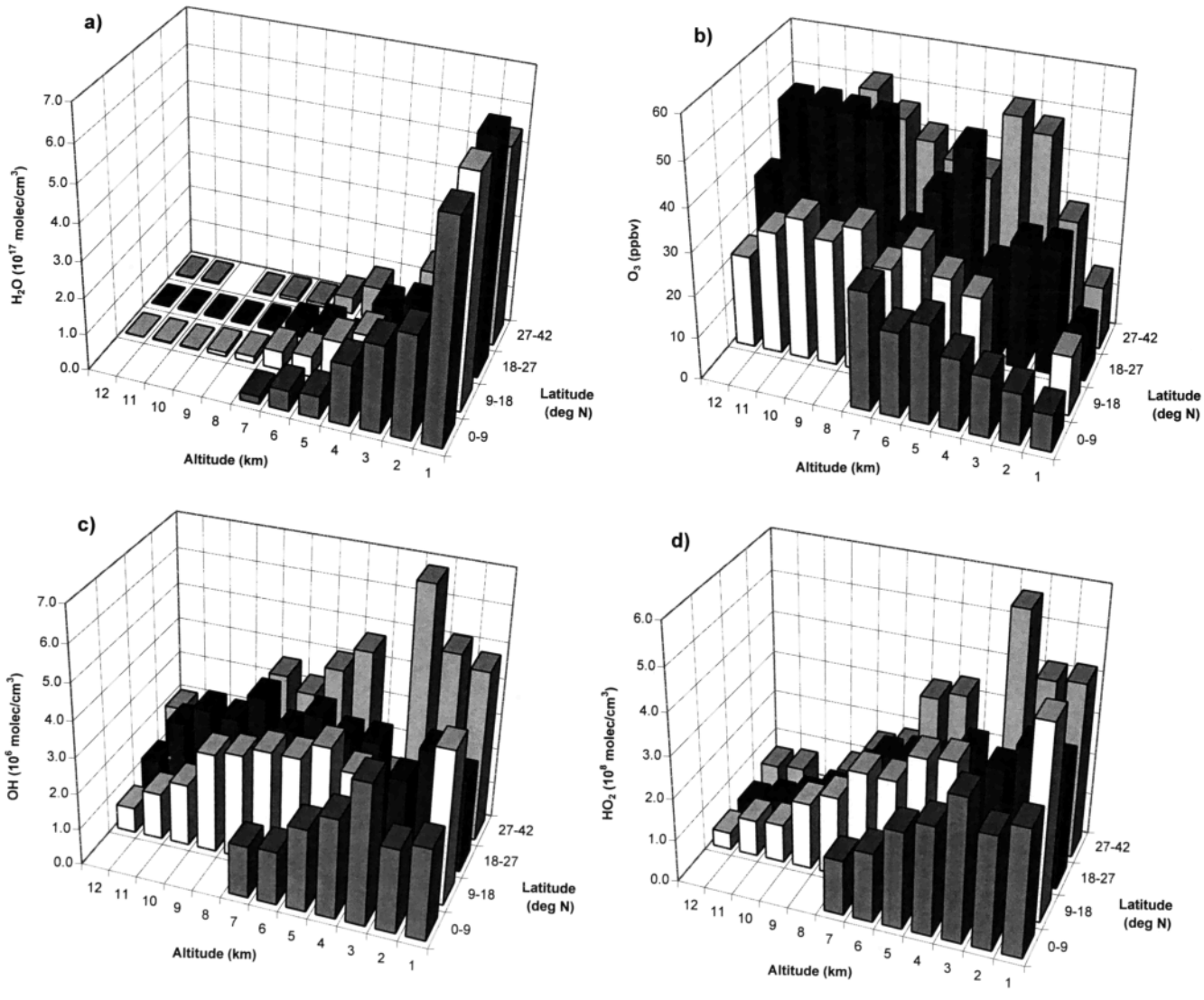

Figure 7. Latitude and altitude distributions of (a) O_3, (b) H_2O, (c) HO_2, (d) OH, (e) CH_3O_2, (f) RO_2, (g) NO, and (h) NO_x. Only data recorded for solar zenith angles of 30° to 60° are shown. Bins without values contained less than three data points.

and very modest decreases in $F(O_3)$ with altitude. A more detailed examination of these trends in terms of specific reaction processes and chemical controlling factors is presented later in the text.

Tables 2a and 2b show a comparison of our "standard" model output with those labeled earlier as "constrained" and "No NMHC." These results show that for nearly all altitudes and latitudes the "constrained" and "No NMHC" $P(O_3)$ values lie within 20% of those for the "standard model." More typically, they are within 10 to 15%. The fact that the "constrained" and "unconstrained" values are very close is not all that surprising considering the good agreement cited earlier in the text between "model-estimated" and experimental observations for H_2O_2 and CH_3OOH. We note that although the agreement was much worse in the case of NO_2, the concentration level of this species was found to have only a minimal impact on HO_x levels and hence on $P(O_3)$. Less expected were the modeling results which compared $P(O_3)$ results "with" and "without" NMHCs. This finding suggests that on average, during the time period of the PEM-West A mission, anthropogenic NMHC emissions had minimal impact on O_3 levels. This point is further expanded on later in the text.

Discussion

$D(O_3)$, $F(O_3)$, and $P(O_3)$ and Chemical Controlling Factor

Figures 8a and 8b indicate that for both the WNPR and the WTNP regions the dominant (e.g., 46-81%) ozone photochemical loss pathway at altitudes ≤ 6 km is the reaction $O(^1D) + H_2O$, (reaction (R4)). Most of the remaining loss is due to the reaction of O_3 with HO_2, (reaction (R9)). For altitudes >6 km, within the WNPR region, (R9) continues to increase in importance such that at altitudes >8 km it defines the single largest O_3 loss. Even so, (R4) and (R10) combined still make up about 50% of the total photochemical loss. In the tropical regime for altitudes up to 8 km, (R4) is always found to be the largest individual O_3 loss process; but collectively, (R9) and (R10) still make up 20 to 45% of the total. For altitudes >8 km,

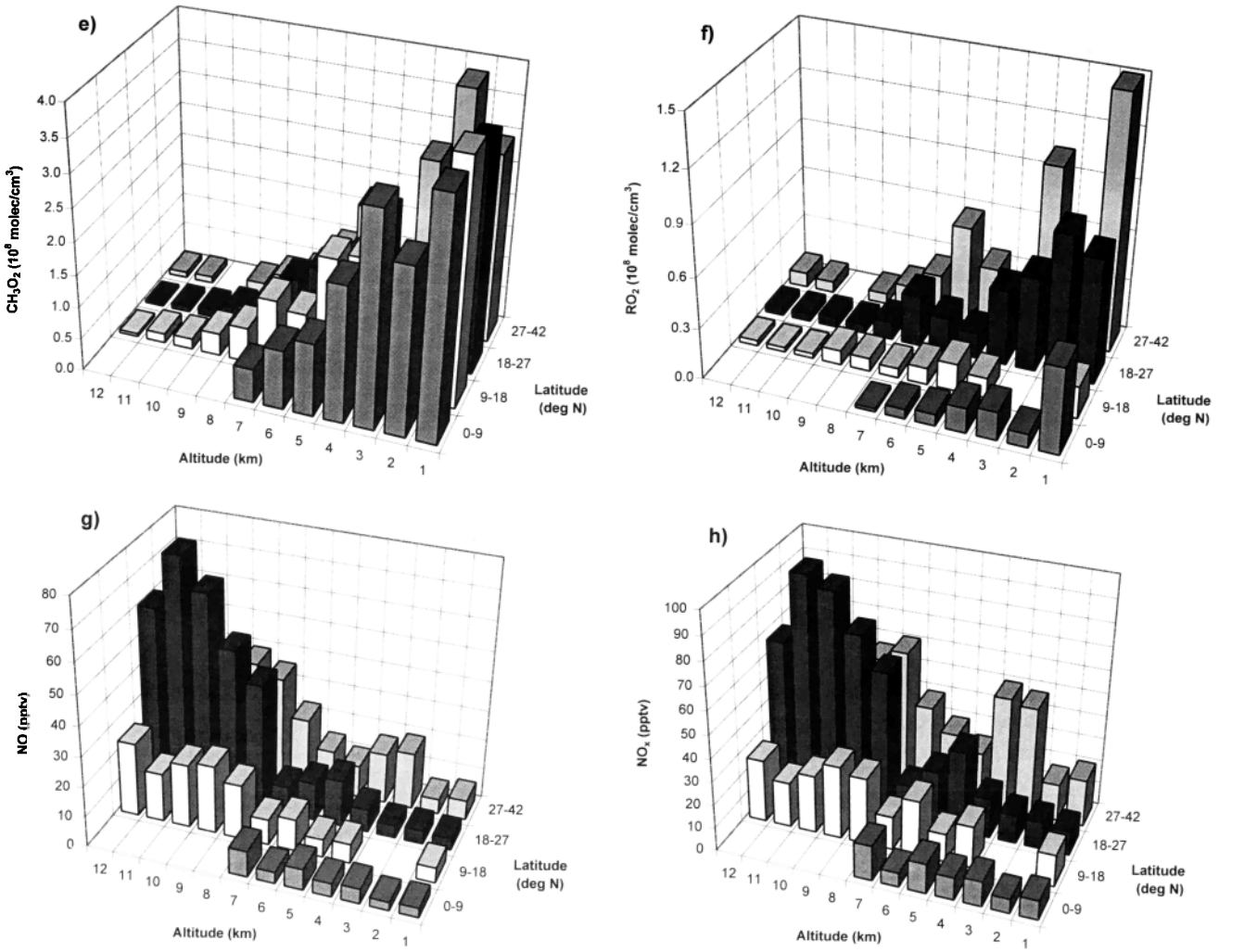

Figure 7. (continued)

(R9) becomes the single largest O_3 loss process, contributing 46% of the total.

As shown in Figure 7b, once above the BL and outside of the latitude band 0°-9°N, the trend in the O_3 mixing ratio with increasing altitude ranges from slightly positive to showing random fluctuations. By comparison, Figures 7a, 7c, and 7d show dramatic drops in H_2O as well as significant decreases in HO_2 and OH levels with increasing altitude. Since both OH and HO_2 are also strongly coupled to H_2O, quite clearly these results point toward the H_2O level as the major chemical factor controlling the altitudinal trend in $D(O_3)$. This point has been further demonstrated here in terms of our exploring the possibility that an empirical equation could be defined that would relate diel values of

Table 2a. Comparison of $P(O_3)$ Values Calculated From Standard, Model, Standard Model Without NMHCs, and Constrained Model for the Latitude Range of 0°-18° N

Alt	Standard[a] molecules/cm^3/s	No NMHC[a] molecules/cm^3/s	Constrained[a,b] molecules/cm^3/s
0-1	-1.0E+06	-1.0E+06	-1.0E+06
1-2	-4.9E+05	-4.9E+05	-4.8E+05
2-4	-4.9E+05	-4.9E+05	-4.8E+05
4-6	-1.4E+05	-1.5E+05	-1.3E+05
6-8	-5.5E+04	-5.8E+04	-6.5E+04
8-10	2.1E+05	2.0E+05	2.3E+05

Read -1.0E+06 as -1.0x10^6.

[a]Results are based on model runs using median input values from the latitude range 0°-18°N.

[b]Constrained species include NO_2, H_2O_2, CH_3OOH, HNO_3, and PAN.

Table 2b. Comparison of $P(O_3)$ Values Calculated From Standard Model, Standard Model without NMHCs, and Constrained Model for the Latitude Range of 18°-42° N

Alt	Standard[a] molecules/cm^3/s	No NMHC[a] molecules/cm^3/s	Constrained[a,b] molecules/cm^3/s
0-1	-3.2E+05	-3.8E+05	-4.0E+05
1-2	-1.5E+06	-1.5E+06	-1.5E+06
2-4	-5.2E+05	-5.7E+05	-5.5E+05
4-6	-1.1E+05	-1.3E+05	-1.4E+05
6-8	3.2E+05	2.9E+05	2.9E+05
8-10	3.7E+05	3.4E+05	3.3E+05
10-12	2.7E+05	2.2E+05	3.0E+05

[a]Results are based on model runs using median input values from the latitude range 18°-42° N.

[b]Constrained species include NO_2, H_2O_2, CH_3OOH, HNO_3, and PAN.

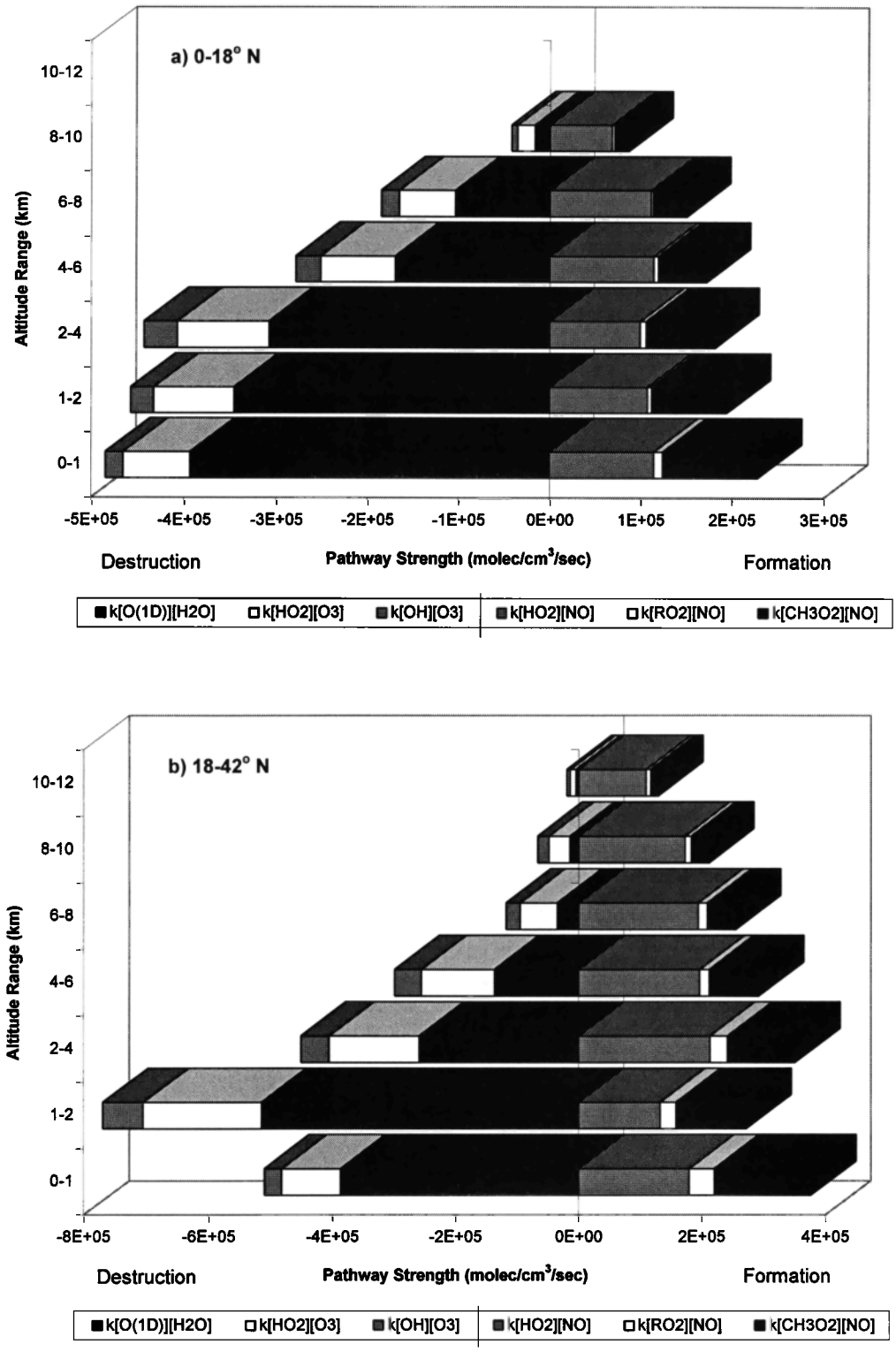

Figure 8. Ozone destruction and formation pathways for the latitude ranges of (a) 0°-18°N and (b) 18°-42°N.

$D(O_3)$ to O_3 and H_2O, e.g.,

$$D(O_3) = \left(\frac{O_3}{M}\right) x\,(1.03 \times 10^5) \times [H_2O]^{.767} \qquad (4)$$

In equation (4) both $[H_2O]$ and [M] have units of molecules/cm^3, $[O_3]$ has units of parts per billion by volume (ppbv), and $D(O_3)$ has units of ppbv/d. Equation (4) suggests that there is a near linear dependence on the concentration of H_2O. A regression plot of diurnally averaged model values of $D(O_3)$ versus those estimated from equation (4) gave an R^2 value of 0.97.

Concerning O_3 formation, Figures 8a and 8b show that when at altitudes of $\leq$4 km, for both the WNPR and the WTNP regions, the two major formation processes are (R5), reaction of NO with HO_2, and (R6), reaction of NO with CH_3O_2. For altitudes >4 km (R5) becomes the dominant

process (e.g., 55 to 85%), with smaller contributions coming from (R6). At all altitudes and all latitudes the contribution from NMHCs, in the form of (R7), is seen as being no more than 11%. Thus this evaluation further confirms our earlier conclusion that overall NMHC emissions were of minor importance as ozone precursors during the sampling time period of PEM-West A.

Given that both HO_2 and CH_3O_2 radical levels decrease systematically with altitude (e.g., Figures 7d and 7e) and that $F(O_3)$ displays only a weak negative trend with altitude (e.g., Figure 6a), NO and peroxy radicals emerge as the major chemical factors controlling the trend in $F(O_3)$. Of course, peroxy radicals are themselves chemically coupled to H_2O. This point is illustrated quite nicely in the form of Figures 7a, 7d, and 7e which show large decreases in the levels of H_2O and peroxy radicals with altitude. Figures 7g and 7h also show that there is a concomitant increase in the mixing ratios of NO and NO_x (i.e., factors of 3 to 20). Although the latter trend is present at all latitudes, the WNPR region clearly shows the largest percent increase.

As in the case of $D(O_3)$, we have also found that diel values of $F(O_3)$ can be related to measured chemical parameters and the estimated quantity, NO_x, by means of equation (5):

$$F(O_3)=\left(\frac{NO_x}{M}\right) \times \{2.87 \times 10^{17} \times \ln\left(\frac{H_2O}{O_3}\right) - 2.47 \times 10^{18}\} \quad (5)$$

here [M], $[O_3]$, and $[H_2O]$ have units of molecules/cm^3, $[NO_x]$ has units of pptv, and $F(O_3)$ has units of ppbv/d. Not surprisingly, equation (5) shows a linear dependence on NO_x but also indicates a logarithmic dependence on the ratio H_2O/O_3. The dependence on H_2O most likely reflects the requirement for a HO_x radical source, whereas the inverse dependence on O_3 very likely reflects losses of HO_x radicals via (R9) and (R10) as well as shifts in the partitioning of NO_x toward NO_2. The latter shift decreases the rate of processes (R5), (R6), and (R7). Model sensitivity tests in which all input variables but O_3 were held constant revealed a similar negative effect on $F(O_3)$. A regression plot of diurnally averaged $F(O_3)$ model values versus those estimated from equation (5) resulted in an R^2 value of 0.98.

The central role of NO in O_3 formation demonstrated in this analysis represents further confirmation of conclusions reached in earlier photochemical studies [e.g., *Liu et al.*, 1980, 1987, 1992; *Ridley et al.*, 1987; and *Chameides et al.*, 1987, 1989]. Unique to this study are the specific results for the western North Pacific, a region heretofore uninvestigated.

$P(O_3)$ and Air Mass Type

As discussed in the previous text, NO and H_2O are two of the key chemical parameters that appear to most influence the trends in $D(O_3)$ and $F(O_3)$. For example, at altitudes <6 km, high levels of H_2O and correspondingly low levels of NO lead to values of $D(O_3)$ that typically exceed $F(O_3)$,

Table 3. Air Mass Designation Codes

Investigator	Code	Description
Gregory et al.	NPFT	North Pacific, free troposphere
	SPFT	South Pacific, free troposphere
	NPML	North Pacific, fixed layer
	SPML	South Pacific, fixed layer
Talbot et al.	CS<2,7-12	continental south, <2 days from Pacific rim, 7-12 km
	CN<2,<2	continental south, <2 days from Pacific rim, <2 km
	CN>2,7-12	continental north, >2 days from Pacific rim, 7-12 km
	CN<2,7-12	continental north, <2 days from Pacific rim, 7-12 km
	CN<2,2-7	continental north, <2 days from Pacific rim, 2-7 km
	CS>2,2-7	continental south, >2 days from Pacific rim, 2-7 km
	CS<2,2-7	continental south, <2 days from Pacific rim, 2-7 km
This Work	CN<2,<1	continental north, <2 days from Pacific rim, <1 km
	CN<2,7-12,CC	continental north, <2 days from Pacific rim, 7-12 km, continental convection
	CN>2,7-12,MC	continental north, >2 days from Pacific rim, 7-12 km, marine convection
	typhoon	influenced by either Typhoon Mireille or Orchid
	MS,7-12,IC	marine south, 7-12 km, island convection
	MN,7-12	marine north, 7-12 km
	MS,7-12	marine south, 7-12 km
	CN<2,1-7	continental north, <2 days from Pacific rim, 1-7 km
	MN,1-7	marine north, 1-7 km
	MS, 1-7	marine south, 1-7 km
	MS,0-1	marine south, 0-1 km
Browell et al.	CO-C	convective outflow-continental
	BK	background air
	CO	convective outflow
	HPLU	high ozone plume
	CP	clean pacific air
	NS	near surface air
Smyth et al.	0.52,2-7	median for the lower third of C_2H_2/CO values from 2-7 km
	0.91,2-7	median for the middle third of C_2H_2/CO values from 2-7 km
	1.75,2-7	median for the upper third of C_2H_2/CO values from 2-7 km
	0.60,7-12	median for the lower third of C_2H_2/CO values from 7-12 km
	1.25,7-12	median for the middle third of C_2H_2/CO values from 7-12 km
	1.74,7-12	median for the upper third of C_2H_2/CO values from 7-12 km

resulting in negative values of $P(O_3)$. For altitudes above 6 km, the reverse situation is found. Water levels are routinely very low; and levels of NO, although highly variable, typically are large enough to result in $F(O_3)$ values that exceed $D(O_3)$. Thus positive values of $P(O_3)$ are found. Here we examine the trend in $P(O_3)$ from a more synoptic perspective. $P(O_3)$ was selected for this exercise since it is this quantity that is most sensitive to changes in environmental conditions.

The air classification scheme used in this analysis (see Table 3) is similar to that described by *Gregory et al.* [this issue] and *Talbot et al.* [this issue] with one important change. We have further subdivided several of their classifications to indicate the presence of deep convection. As noted earlier in our discussion of individual flight tracks, on numerous occasions the high-altitude levels of several trace gases were significantly influenced by deep convection. Thus the scheme shown in Table 3 reflects our conclusion that deep convection was a frequent source of elevated levels of NO_x for altitudes above 6 km. As noted earlier, these elevated levels of NO_x were strongly correlated with our calculated values of $P(O_3)$.

To identify deep convection events, we took an approach very similar to that described earlier in our analysis of flights 10, 12, and 15. However, in addition to the meteorological and chemical data presented in that analysis, we also found it useful to include the chemical tracers: O_3, H_2O, DMS, SO_2, C_2H_2, C_2H_6, CH_4, PAN, CH_3I, $(NO_x)_{mc}$, and NO_y. Again, as seen from Table 3, this has led to our identifying a total of 11 air mass classes. Each of these classifications is based on our having identified significant data segments from two or more flights, each showing similar characteristics. Figure 9 shows these 11 classifications separated according to their respective median values of $P(O_3)$. Also shown as a function of $P(O_3)$ values are the classifications reported by *Gregory et al.* [this issue], *Talbot et al.* [this issue], *Smyth et al.* [this issue], and *Browell et al.* [this issue].

A survey of Figure 9 reveals that clean BL marine air (e.g., Gregory et al's. NPML and SPML; this work's (MS, 0-1); and Browell et al's NS) shows the lowest values of $P(O_3)$. For this case, values are observed to range from -5×10^5 to -1×10^6 molecules/cm^3/s. By comparison, lower free-tropospheric air parcels (i.e., 1-7 km), either of continental or marine origin, tend to show values that range from moderately negative to zero (e.g., Talbot et al's. (CS<2, 2-7), (CS>2, 2-7), and (CN<2, 2-7); this work's (MS, 1-7) and (MN, 1-7); and Browell et al's. CP). Zero to weakly positive values of $P(O_3)$ begin to emerge for upper free-tropospheric air (i.e., $z \geq 7$ km) of marine origin (see Gregory et al's. SPFT and NPFT; Browell et al's. CO; and this work's (MS, 7-12) and (MN, 7-12)).

Significant positive values of $P(O_3)$ (i.e., $\geq 2.0\times10^5$ molecules/cm^3/s) are observed for air parcels labeled here as relatively fresh BL air of continental origin or upper free-tropospheric air (particularly upper free-tropospheric air that had been influenced by deep convection). This group includes: Talbot's (CN< 2, 7-12), (CN> 2, 7-12), (CN< 2,< 2), and (CS<2, 7-12); this work's (MS, 7-12, IC), (CN>2, 7-12, MC), (CN<2, 7-12, CC), and (CN<2, 0-1), and Browell et al's. HPLU, CO, BK, and CO-C designations. As noted earlier, Talbot did not attempt to explicitly identify in his classification scheme air parcels that had been convectively processed; however, these parcels would have been components of all of his 7 to 12 km designations.

Of some interest also is the fact that Browell et al's identification of convectively influenced air parcels was quite different than that used in this analysis. These investigators based much of their interpretation on O_3 and aerosol measurements as recorded with an airborne differential absorption lidar (DIAL) instrument. This information was then further supplemented with independently evaluated potential vorticity profiles. Despite the difference in classification criteria, these authors' convective outflow designations seem to agree well with those from this work. For example, high $P(O_3)$ values are observed for continental convective outflow cases (CO-C), and weakly positive values are seen for marine-convective outflow (CO).

Smyth et al.'s [this issue] values for the ratio C_2H_2/CO are also shown in Figure 9. For purposes of comparing with $P(O_3)$, we have grouped Smyth et al's. results into six bins. These bins have been defined by first separating their results into lower free-tropospheric and upper free-tropospheric groupings. Each of these groups, in turn, was subdivided into three subgroups based on the magnitude of the C_2H_2/CO ratio. These subgroups are identified in Figure 9 by their median values of the ratio C_2H_2/CO. They define air mass types that range from well-processed air (i.e., near background) to relatively fresh anthropogenic emissions. The corresponding values of $P(O_3)$ are shown as ranging from -2×10^5 to +3.5×10^5 molecules/cm^3/s. As seen from Figure 9, the observed trend appears to parallel that predicted from the other air mass classification schemes. For example, upper tropospheric values of the ratio are seen as having positive values of $P(O_3)$; whereas lower free-tropospheric ratios correlate with negative $P(O_3)$ values. Within an altitude grouping, one might also expect that the higher the value of the ratio the higher the value of $P(O_3)$. This, in fact, is what is observed for the high-altitude block. On the other hand, for the lower free-tropospheric grouping the results appear to be somewhat anomalous. In this case the highest ratio does not correlate with the highest $P(O_3)$ value; however, the separation between $P(O_3)$ values for the three different ratios is also seen to be quite small and probably lies well within the uncertainties of the measurements and/or modeling calculations.

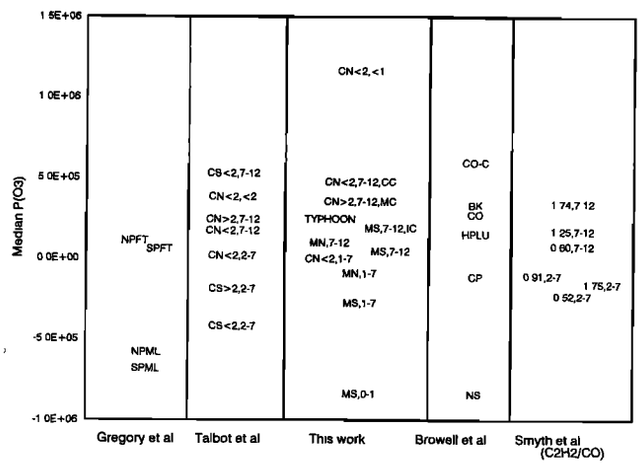

Figure 9. Median values of $P(O_3)$ for five different air mass classifications. Definitions for individual codes are given in Table 3.

Trends in Other Photochemical Parameters

Critical-NO and NO_x. That level of NO at which photochemical production of ozone from processes (R5), (R6), and (R7) is exactly balanced by photochemical ozone destruction due to processes (R4), (R9), and (R10) defines the "critical" NO level. Thus it represents the NO level where $P(O_3)$ changes sign.

In the current analysis, values of $NO_{(crit)}$ were estimated based on median values for all model input parameters. These evaluations were carried out for 13 altitude/latitude data bins as shown in Table 4. The results show $NO_{(crit)}$ values ranging from 6 to 17 pptv, with the median value being close to 11 pptv. No simple trend appears to be present in these results except perhaps in the case of the WNPR region. Here it is seen that for altitudes above 1 km there is a trend of decreasing $NO_{(crit)}$ values with increasing altitude.

On average, ambient NO levels for altitudes <4 km are found to be 1.5 to 3 times lower than $NO_{(crit)}$; whereas for altitudes above 8 km they tend to be 1.5 to 4 times higher. Although the higher $NO_{(crit)}$ values are similar to those reported for other Pacific databases [e.g., *Ridley et al.*, 1987; and *Chameides et al.*, 1989], the low values at the highest altitudes seem to be somewhat anomalous. These low values, however, are found to be closely correlated with very low values for $D(O_3)$ which, as noted earlier in the text, reflects the very low H_2O levels found at these altitudes.

In contrast to $NO_{(crit)}$ values, with the exception of one or two low-altitude points, Table 4 shows that for both latitude ranges, $NO_{x(crit)}$ generally decreases with increasing altitude. The stronger trend in $NO_{x(crit)}$ most likely reflects this parameter being a more conserved quantity than NO. As noted earlier in the text, the partitioning of NO_x between NO and NO_2 is a strong function of altitude.

From Table 4 the values of $NO_{x(crit)}$ can be seen ranging from 7 to 50 pptv, giving a median value of 20 pptv. In the only other study in the Pacific for which $NO_{x(crit)}$ values were evaluated (e.g., [*Liu et al.*, 1992], levels of 55 pptv were reported for an altitude of 2-3 km. At a similar altitude, the PEM-West A results suggest $NO_{x(crit)}$ levels of between 25 and 39 pptv.

NO_x lifetime. Lifetime estimates for NO_x as a function of altitude and latitude are presented in Table 4. For these evaluations the daytime gas phase reaction of NO_2 with OH was taken as the only major loss process for NO_x. The results indicate that lifetimes for NO_x can range from 1 to 1.5 days for low-altitudes and 3 to 9 days at high-altitudes (i.e., 8-12 km). By contrast, high-altitude lifetime estimates for NO_2 fall into the range of 1 to 2 days. The difference between these two estimates reflects the large shift in the partitioning of NO_x toward NO at high-altitudes. This shift is due both to the much slower rate of conversion of NO to NO_2, via its reaction with O_3, and to a somewhat enhanced NO_2 photolysis rate at high-altitudes.

The extended lifetime for NO_x at high-altitudes suggests that deep convection events 3000 to 4000 km inland from the coast could still represent potentially important sources of NO_x for the western Pacific. Similarly, taking the nominal high-altitude fall-season winds observed during PEM-West A as representative (i.e., 55 km/h), within 9 days significant amounts of NO_x, generated from deep convection near the Asian coast, could virtually cross the entire Pacific. Although large mixing factors would be involved, considering the absence of other major primary NO_x sources over the open ocean, deep convection along the Asian coast could prove to be one of the more important sources of NO_x to the North Pacific. In fact, evidence supporting the importance of long-range transport of high-altitude NO_x can be found in the NO data recorded in the tropics (see, for example, earlier discussion under "Ozone Photochemical Trends: Flight Track Analysis").

NO_x-O_3 chain length and unit production rate. The NO_x-O_3 chain length may be defined as the number of O_3 molecules produced photochemically per NO_x molecule oxidized. *Liu et al.* [1987] were the first investigators to discuss this quantity and, subsequently, labeled it "ozone production efficiency" [*Fehsenfeld and Liu*, 1993]. We will here refer to this quantity as the NO_x-O_3 chain length. Under quasi steady state conditions it can be estimated from equation (6):

Table 4. Assessment of Critical Parameters in the Formation of Ozone

Latitude °N	Altitude km	$(NO)_{meas}$[a] pptv	Critical NO[b] pptv	$(NO_x)_{mc}$[c] pptv	Critical NO_x[d] pptv	NO_x Lifetime days	NO_x-O_3 Chain Length[e]	ΔP[f], ppbv-O_3/ pptv-NO_x day
0-18	0-1	4	12	11	33	1.8	140	0 .078
0-18	1-2	4	9	10	18	1.6	131	0 .081
0-18	2-4	5	12	12	25	1.4	102	0 .075
0-18	4-6	7	10	15	19	1.8	122	0 .068
0-18	6-8	10	11	17	19	2.4	142	0 .059
0-18	8-10	15	10	20	14	6.2	246	0 .039
18-42	0-1	7	9	20	24	1.6	108	0 .068
18-42	1-2	5	17	17	50	1.1	73	0 .065
18-42	2-4	10	16	28	39	1.4	86	0 .061
18-42	4-6	14	16	32	34	1.5	83	0 .054
18-42	6-8	24	12	47	20	2.6	105	0 .040
18-42	8-10	43	11	66	17	3.2	95	0 .029
18-42	10-12	62	6	73	7	8.9	209	0 .023

[a]$(NO)_{meas}$, Median-measured NO level.
[b]Critical NO, NO level at which photochemical production and destruction of O_3 are in balance.
[c]$(NO_x)_{mc}$, 24-hour average calculated NO_x level.
[d]Critical NO_x, NO_x level at which photochemical production and destruction of O_3 are in balance.
[e]NO_x-O_3 chain length, number of O_3 molecules produced photochemically per NO_x molecule oxidized.
[f]ΔP, the change in O_3 formation rate (ppbv/d) for a given increment of NO_x (pptv).

$$CL = \frac{k_5[HO_2]+k_6[CH_3O_2]+k_7[RO_2][NO]}{k_{11}[OH][NO_2]} \quad (6)$$

The numerator in this equation consists of what earlier was defined as $F(O_3)$, and the denominator represents the loss of NO_x due to the daytime reaction of NO_2 with OH, i.e., (R15):

(R15) $$NO_2 + OH + M \longrightarrow HNO_3$$

Although other possible loss channels could be considered (i.e., NO_3/N_2O_5/aerosol nighttime chemistry), because of a lack of quantitative details concerning these loss processes [*Wayne et al.*, 1991], we have restricted NO_x losses to reaction (R15) only. (Estimates of the possible error associated with this approximation indicate that it is probably less than a factor of 2 for PEM-West A conditions.)

The "primary" chain length as defined by equation (6) is important in that given adequate time, it defines the amount of O_3 that could be photochemically produced from each NO_x molecule released into the troposphere before being converted into a more stable NO_y form. In the lower troposphere, because of the short lifetime of both NO_x and the product HNO_3, the primary chain length can be used in combination with known NO_x emission rates to directly estimate O_3 production [*Liu et al.*, 1987; *McKeen et al.*, 1991]. However, in the upper free-troposphere, because of a much extended lifetime for HNO_3, this species may be recycled back to NO_x to initiate new O_3 production. Thus as reported by *Liu et al.* [1995], the "ensemble chain length" for O_3 production is defined in terms of the product of the primary chain length and the total number of times a given NO_x molecule cycles through HNO_3 or some other NO_y species (for additional detail on this point see discussion under "NO_x Sources"). This means that to quantitatively evaluate the contribution of a given NO_x source to photochemical O_3 formation, both the primary chain length and the recycling efficiency must be known. As discussed below, the magnitude of both of these terms can be a function of altitude as well as other factors such as the NO_x concentration itself.

The effect of the NO_x concentration on chain length becomes apparent once it is recognized that elevated NO_x not only promotes reactions (R5), (R6), and (R7) but also leads to a reduction in HO_x radical levels via the enhancement of reactions of the type (R15). *Liu et al.* [1987] have reported both modeling and field results that address this issue for surface summertime conditions at northern midlatitudes. In fact, their results indicate that NO_x levels at 10 pptv should generate 8 times more O_3 per molecule of NO_x oxidized than at 10 ppbv, given similar chemical and physical environmental conditions. Still more recent observations and corroborating modeling studies have further demonstrated the general soundness of this thinking, particularly as related to high NO_x mixing ratios (e.g., *McKeen et al.* [1991]). Very few studies have been reported for NO_x mixing ratios in the range involving the largest nonlinearity in O_3 production, e.g., 10 to 1000 pptv and altitudes not near the surface.

Shown in Table 4 are the "chain length" estimates for the PEM-West A data. For the altitude interval of 0 to 12 km, the corresponding NO_x levels are seen falling into the range of 10 to 70 pptv. Quite important, though, over this same altitude interval ambient chemical and physical conditions are also observed to change significantly (e.g., see Figures 7a-7h). As a result, changes in the partitioning of NO_x between NO and NO_2 are found to have a noticeable influence on the estimated value of CL. For example, for both the WTNP and the WNPR regions, NO_x mixing ratios are seen increasing by factors of 2 to 3.5 over the altitude range of 0-12 km. This might suggest that modest decreases in CL should have been observed. But as seen from Table 4, no systematic trend in CL as a function of altitude is observed, although maximum values do tend to occur at the highest altitudes, i.e., 8-12 km. We conclude from this that for the case of the PEM-West A data the value of the NO_x-O_3 chain length at different altitudes was controlled by both the partitioning of NO_x as well as by the NO_x mixing ratio. This point was further illustrated in this work by carrying out high-altitude model simulations in which all chemical and physical parameters were held fixed but NO_x. In this case for the altitude interval of 8-10 km, variations of plus and minus a factor of 3 resulted in a total variation in CL of up to a factor of 4.5. As noted earlier, changes in the level of NO_x are inversely related to changes in CL.

Although the primary chain length may give an indication of O_3 formation from one NO_x molecule before that molecule is oxidized, it is also of some value to examine the near term, diel, O_3 production efficiency from NO_x. We will here refer to this quantity as the O_3 production per unit NO_x per day and give it the symbol ΔP, as per *Liu et al.* [1987]. Thus ΔP is simply CL/τ_{NOx}. Liu et al. have reported modeling results for summer surface conditions which suggest that ΔP should be nearly independent of NO_x at levels less than 1 ppbv when all other parameters are held constant. As shown in Table 4, we report ΔP results for the PEM-West A data for surface conditions as well as for the middle and upper free-troposphere. The 0 to 12 km results show that for the WTNP and the WNPR regions, ΔP decreases with altitude by factors of 2 to 3. Furthermore, this decrease with altitude appears to be mostly driven by an increase in the NO_x lifetime which, in turn, reflects changes in the partitioning of NO_x as well as changes in HO_x levels. For example, sensitivity tests at 8-10 km involving variations in NO_x of plus and minus a factor of 3 show that the average change in ΔP was only a factor of 1.4.

Thus based on actual high-altitude observations, the PEM-West A results suggest that for the remote troposphere, given adequate time, one gets only slightly more mileage from a given NO_x molecule at high-altitude than for altitudes near the surface. Furthermore, because of the long reaction times involved at high-altitude, transport processes become quite important in defining the influence of any newly formed O_3 on actual observed O_3 levels. By contrast, in the remote troposphere diel O_3 production per unit NO_x is significantly higher at low-altitudes. However, insofar as $F(O_3)$ is concerned, the lower value of ΔP at high-altitudes is typically compensated by much higher levels of NO_x and by the strong partitioning of NO_x in favor of NO.

NO_x Sources

The results from this study as well as those from several earlier studies [e.g., *Liu et al.* 1980; *Chameides et al.* 1987, 1989; and *Ridley et al.* [1987] have shown that NO is the rate-limiting precursor in the formation of O_3. The issue of

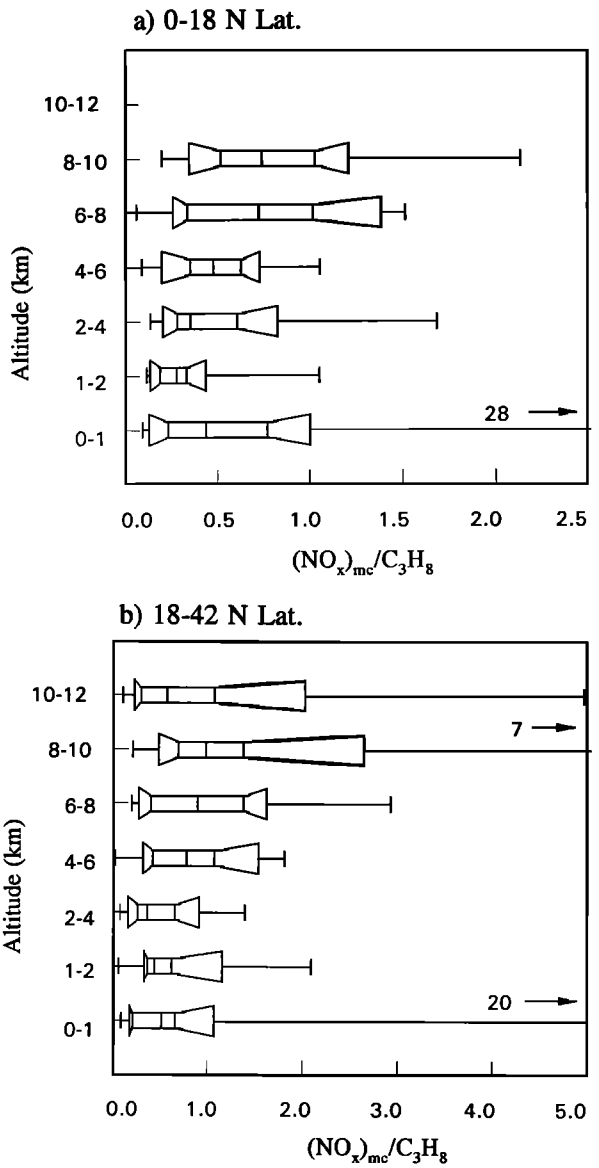

Figure 10. Box-Whisker plot of the ratio $(NO_x)_{mc}/C_3H_8$ versus altitude for the latitude ranges (a) 0°-18°N and (b) 18°-42°N. Whiskers encompass the entire range of the data, while boxes indicate the 10th, 25th, 50th (median), 75th, and 90th percentile of the data.

NO_x sources therefore is centrally important to understanding the tropospheric O_3 budget. For the western Pacific, possible "primary" NO_x sources would include continental outflow of industrial emissions and/or biomass burning, stratospheric intrusions, lightning, and aircraft emissions (see, for example, *Fehsenfeld and Liu,* [1993] and references therein). In addition, as discussed earlier in the text under "NO_x-O_3 chain length," there can also be recycling of NO_y to yield new NO_x, this source being labeled "secondary" NO_x [e.g., *Liu et al.*, 1987; *Chatfield and Crutzen.*, 1990; *Jacob et al.*, 1992; *Singh et al.*, 1992; *Fan et al.*, 1994; *Singh et al.*, 1994]. Aspects of each of these sources have been addressed in several other PEM-West A papers [e.g., *Singh et al.*, this issue; Liu et al., this issue; *Kondo et al.* this issue; *Davis et al.*, this issue; *Liu et al.*, this issue]. Thus the primary focus of this text will be to compare and summarize some of the more important findings of these efforts.

Figures 10a and 10b show altitude versus $(NO_x)_{mc}/C_3H_8$ plots where the data have been binned to help visualize the underlying trends. In this case, the results show quite clearly that for both the WNPR and the WTNP regimes, median values of the ratio $(NO_x)_{mc}/C_3H_8$ increase with increasing altitude by nearly a factor of 2. Since the major source of propane is combustion and natural gas emissions [*Blake et al.*, 1992, 1994, this issue] and the lifetime of propane is 3-5 times longer than NO_x, such profiles would seem to argue in favor of the major source of NO_x being located at high-altitudes. Similarly, when the ratio $(NO_x)_{mc}/C_3H_8$ is plotted against a second ratio, C_2H_2/CO, as shown in Figures 11a and 11b, the trend is one in which increasing values of $(NO_x)_{mc}/C_3H_8$ are observed for decreasing values of C_2H_2/CO. As discussed by *Smyth et al.* [this issue], the latter ratio can be a useful indicator of the degree of processing that an air parcel has undergone after being released from a combustion source. This means, then, that the larger the value of this ratio the closer the sampled air parcel must be to the original source of combustion. For the specific case of PEM-West A the high-altitude results would again appear to be most consistent with there being a major nonsurface source of NO_x. *Singh et al.*, [this issue] arrived at a similar conclusion. These authors, using a similar type analysis as shown in Figures 10a-11b but in conjunction with three-dimensional modeling results, have suggested that no more than 20% of the high-altitude NO_x could be attributable to surface sources. In an independent three-dimensional modeling effort, focused only on the WNPR region, *Liu et al.* [this issue] arrived at a very similar conclusion; that is, surface sources account for <25% of the high-altitude NO_x. However, this still leaves open the question of the nature of the remaining (75-80%) high-altitude NO_x source. As noted above, the possibilities include near-term releases from "primary" sources in the form of lightning, aircraft emis-

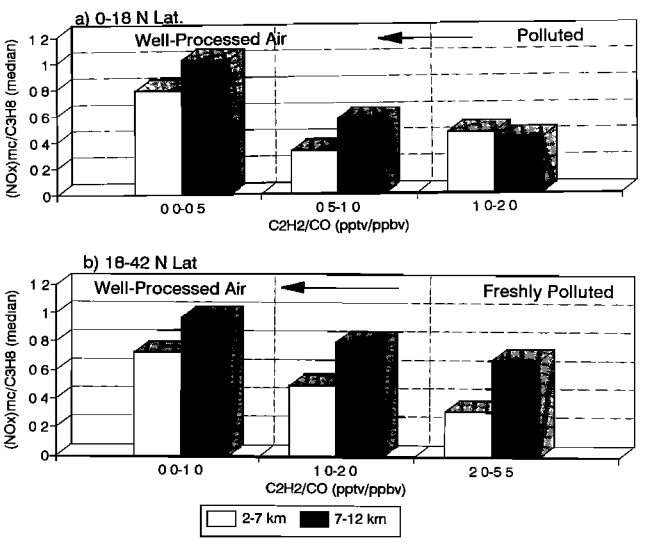

Figure 11. Bar graphs showing the median value of the ratio $(NO_x)_{mc}/C_3H_8$ versus the "air mass processing" ratio, C_2H_2/CO. Data are separated into two altitude ranges, 2-7 km and 7-12 km.

sions, and stratospheric intrusions as well as NO_x from "recycled" NO_y, the NO_y itself being defined by some unknown mix of primary NO_x sources. Operationally, the determination of the relative contributions from these two general classes of NO_x can be quite problematic, although tracer analysis in conjunction with modeling studies can frequently prove insightful.

D. Davis et al. [manuscript in preparation, 1995], for example, report a chemical tracer scheme in which semiquantitative evaluations of NO_x from deep convection associated with lightning were carried out based on individual convective events. Central to their approach was the recognition that during the PEM-West A mission typical free-tropospheric background levels of C_3H_8 were quite low. As noted earlier in the text, the sources of C_3H_8 are all surface in origin. Under these conditions the ratio C_3H_8/NO_x can potentially be used as an indicator of the relative contributions from lightning and surface emissions. Based on extensive surface data collected in the southeastern United States plus low-altitude observations during PEM-West A of combustion plumes coming off the coast of China, Japan, and Taiwan, the average "downwind from source" value for this ratio was evaluated at 3.0 $\pm$1.0. Since the lifetime of C_3H_8 is 3-5 times greater than NO_x, direct observations of the C_3H_8/NO_x ratio in high-altitude convective-outflow plumes made possible upper limit estimates of the fraction of NO_x attributable to surface emissions versus lightning. Their results suggested that during PEM-West A better than 71% of the NO_x observed in these individual events was attributable to lightning. (Somewhat similar conclusions have been reported in several other airborne field studies [e.g., *Chameides et al.*, 1987; *Ridley et al.*, 1987; *Pickering et al.*, 1993; *Luke et al.*, 1992].)

Liu et al. [this issue], using a three-dimensional mesoscale transport/chemical model, have indicated that for the Pacific rim region, contributions to the NO_y pool for the upper troposphere consisted of stratospheric oxidized N_2O, subsonic aircraft emissions, and lightning/surface emissions. They assign contributions from the first two sources of 25% and 50%, respectively. The rest, 25%, they attribute to lightning and surface emissions derived from deep convection/vertical transport. These authors caution, however, that based on comparisons between model predictions and observations for several other trace gases, their results probably underestimate the contribution from deep convection/vertical transport for this region during the time period of PEM-West A. In yet another independent study, *S. Liu et al.* [manuscript in preparation, 1995] have further investigated the issue of recycled NO_y as a source of NO_x by examining values of the experimentally derived ratio NO/NO_y. In their analysis this ratio was compared against model-predicted ratios. These model-predicted ratios were based on the assumption that the system was at photochemical equilibrium. Since for altitudes above 7 km the experimental ratio was generally found to be smaller than the photochemical equilibrium value, their results suggest that the photochemical conversion of NO_y to NO_x was a major source of NO_x. They further suggest that the most likely form of this NO_y would be HNO_3. This species was indicated to be inefficiently scavenged by upper tropospheric aerosols, particularly ice particles.

D. Davis et al. [manuscript in preparation, 1995], using a time-dependent box model similar to that described in this text, also examined the NO_x-NO_y recycling issue. The approach taken by these authors was to explore what level of NO_x could be supported in the upper free-troposphere, given the reported PEM-West A levels of PAN and HNO_3. Based again on the assumption of photochemical equilibrium, their results indicated that $<12\%$ of the high-altitude NO_x could be explained by the reported measurements of HNO_3 and PAN. However, other evaluations by these authors, in which the NO_y "shortfall" (NO_y-PAN-HNO_3-$(NO_x)_{mc}$) was assumed to have chemical characteristics not too dissimilar from HNO_3, led to a quite different conclusion. The latter results showed that photochemically converted "shortfall" NO_y could explain most of the high-altitude observations for the WTNP regime and $\geq 60\%$ of the observations for the Pacific rim. These investigators caution, however, that their calculations must be viewed in the context of possible major uncertainties in the reported high-altitude values of NO_y (J. Bradshaw, private communication, 1995). Of some concern in this regard, the high-altitude "shortfall" for the PEM-West A WTNP region was $\geq 87\%$, while that for the WNPR regime was $\geq 65\%$. More recently, questions have also been raised about the HNO_3 measurements [*E. Atlas et al.*, manuscript in preparation, 1995]. Finally, the possibility that yet unknown recycling processes, involving HNO_3 or other NO_y species, could alter the model predictions also cannot be totally dismissed.

Concerning the lower troposphere, both the modeling results of *Singh et al.* [this issue], and *Liu et al.* [this issue] tend to show substantial increases in the direct contribution of surface sources to the NO_x pool. These contributions, however, appear to be coming predominantly from industrial or natural sources rather than biomass emissions. In fact, of the low-altitude encounters with plumes showing highly elevated levels of NO_y and NO_x, halocarbon signatures suggest that in no case could the plume be attributed predominantly to biomass burning.

Diurnal Photochemical Trends and Ozone Budgets

The evaluation of the O_3 budget was carried out using diurnal profiles for $D(O_3)$ and $F(O_3)$, as shown in Figures 12a and 12b. Table 5 gives the diurnal average rates for $D(O_3)$ and $F(O_3)$ as estimated from these profiles. The diurnal profiles for $P(O_3)$ are shown in Figures 13a and 13b; the average values of $P(O_3)$ based on these profiles are again given in Table 5. Recall that it is the diurnal average value of $P(O_3)$ that most directly relates to the impact of photochemistry on ambient levels of O_3. From Table 5 we see that in all cases but one the daily change in O_3, either positive or negative, is smaller than 2 ppbv. Thus changes in local ambient ozone levels, as driven by photochemical process, are predicted to have been very gradual.

For the specific case of the tropical marine BL the diurnal average value of $P(O_3)$ is approximately -1 ppbv/d, or about 11% of the typical ambient level. This result is consistent with numerous other analyses of O_3 photochemistry in the tropical Pacific BL [e.g., *McFarland et al.*, 1979; *Liu et al.*, 1983; *Thompson and Lenschow*, 1984; *Piotrowicz et al.*, 1986; *Johnson et al.*, 1990; *Thompson et al.*, 1993]. As discussed by *Singh et al.* [this issue], photochemical destruction via reaction (R4), in combination with weak downward

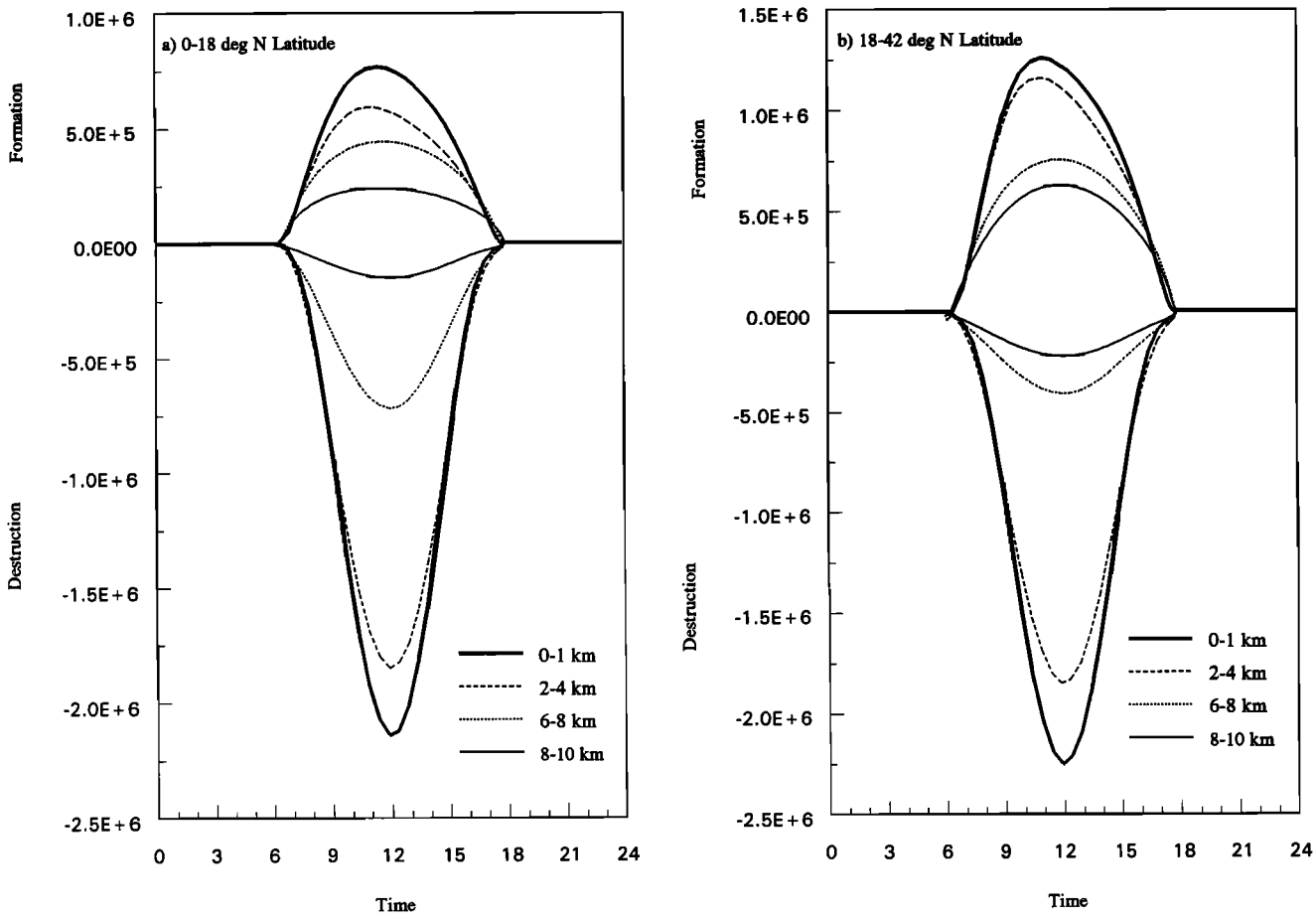

Figure 12. Diurnal profiles of $F(O_3)$ and $D(O_3)$ from TD modeling runs. Profiles are for the latitude ranges (a) 0°-18°N and (b) 18°-42°N.

O_3 transport, is the most likely explanation for the very low values of O_3 observed in the tropics during PEM-West A. On the other hand, at high-altitudes, where $P(O_3)$ values for the Pacific rim region are given as ~ +1 ppbv/d, several ppbv of O_3 could have been generated during the lifetime of O_3.

Figures 14a -14c show the values of $D(O_3)$, $F(O_3)$, and $P(O_3)$ displayed as diurnal-averaged column-integrated quantities. These results clearly identify the free-troposphere as being by far the largest contributor to the North Pacific ozone budget. For example, it can be estimated that the column-integrated O_3 formation and destruction fluxes for the free-troposphere (i.e., 1-12 km) are 5 to 8 times larger than for the marine BL (0-1 km). Thus the PEM-West A data support the earlier conclusions of *Fehsenfeld and Liu* [1993] that photochemical activity within the BL has a minimal impact on the global budget of O_3. Only in the event that significant BL sources of NO_x were present and this NO_x was convectively transported to high-altitudes would the importance of BL NO_x levels to the O_3 budget be enhanced [e.g., *Chatfield and Delany*, 1990; *Pickering et al.*, 1990; *Fehsenfeld and Liu*, 1993].

From Figure 14b we also see that for the WNPR region the O_3 column production flux (i.e., 31×10^{10}

Table 5. Diurnal Averaged Rates for O_3 Formation, Destruction, and Tendency

Altitude Range,km	Latitude Range, 0°-18° N				Latitude Range, 18°-42° N			
	$F(O_3)$, molec/cm^3/s	$D(O_3)$, molec/cm^3/s	$P(O_3)$, molec/cm^3/s	$P(O_3)$, ppbv/d	$F(O_3)$, molec/cm^3/s	$D(O_3)$, molec/cm^3/s	$P(O_3)$, molec/cm^3/s	$P(O_3)$, ppbv/d
0-1	2.28E+05	4.84E+05	-2.56E+05	-0.94	3.76E+05	5.10E+05	-1.34E+05	-0.49
1-2	1.94E+05	4.57E+05	-2.63E+05	-1.11	2.72E+05	7.69E+05	-4.97E+05	-2.05
2-4	1.81E+05	4.43E+05	-2.62E+05	-1.26	3.50E+05	4.51E+05	-1.00E+05	-0.49
4-6	1.72E+05	2.79E+05	-1.07E+05	-0.64	2.92E+05	2.99E+05	-6.64E+03	-0.04
6-8	1.50E+05	1.85E+05	-3.52E+04	-0.24	2.55E+05	1.18E+05	1.37E+05	1.00
8-10	8.64E+04	4.24E+04	4.40E+04	0.40	2.12E+05	6.66E+04	1.45E+05	1.30
10-12					1.29E+05	1.92E+04	1.10E+05	1.44

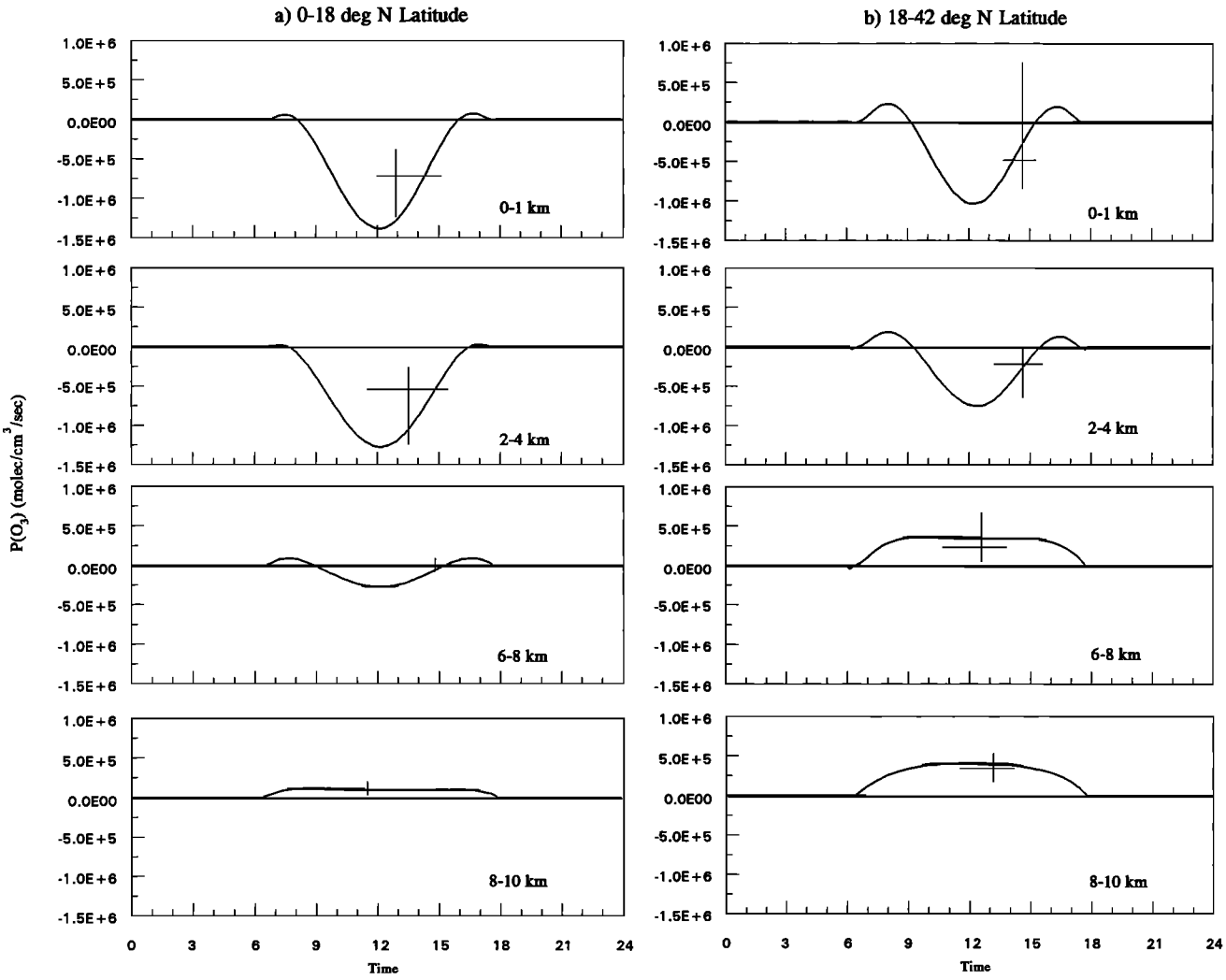

Figure 13. Diurnal profiles of $P(O_3)$ from TD modeling runs. Profiles are for the latitude ranges (a) 0°-18°N and (b) 18°-42°N.

molecules/cm^2/s) is about a factor of 6 greater than the average Northern Hemisphere (NH) stratospheric O_3 flux [e.g., *Gidel and Shapiro,*1980; *Mahlman et al.*, 1980]. Similarly, the column photochemical destruction is nearly 6 times larger than the O_3 deposition flux to the ocean [e.g., *Kawa and Pearson*, 1989; *Lenschow et al.*, 1982].

The near balance between column photochemical production and destruction (i.e., Figure 14b) suggests that O_3, as observed in the WNPR region during PEM-West A, was near steady state. This result is not all that surprising when considering the column average lifetime of O_3. For example, the WNPR region, based on a column-integrated O_3 concentration of 5.4×10^{17} molecules/cm^2, is estimated to have an average column lifetime of only 20 days. Equally important, we estimate that the observed seasonal change in column O_3 for this region is no more than 15% [*Fishman et al.*, 1990]. The latter estimate, however, assumes that the O_3 distribution observed during PEM-West A is consistent with those of *Fishman et al.* [1990]. In fact, an analysis by *Gregory et al.* [this issue] has confirmed that this is the case for both the WNPR and the WTNP regions.

Since the column average lifetime of O_3 for the tropical regime is estimated to be even shorter (i.e., 16 days) than that for the WNPR region and the seasonal changes are also smaller, one would expect that steady state conditions would also prevail in the former regime. But this requires that the column-integrated budget for O_3 be approximately balanced. Figure 14a, however, shows that the 0 to 10 km column destruction rate exceeds production by about 80%, leaving a significant O_3 deficit of nearly 12×10^{10} molecules/cm^2/s. At these low-latitudes it is highly unlikely that any direct influx of O_3 from the stratosphere could balance this deficit. It is possible, though, that an influx of O_3-rich midlatitude tropospheric air could compensate for this deficit.

An alternative hypothesis is that the deficit could be balanced by additional O_3 photochemical production at altitudes between 10 km and the tropopause. To explore this possibility, model simulations were carried out in which increasing levels of NO were added to altitudes ranging from 10 km to the tropopause (i.e., 17 km). The results show that increases in O_3 formation start leveling off as NO mixing ratios approach 150 pptv. Based on the "flight track analysis" for flight 15 presented earlier in the text such elevated levels of NO do not appear to be unrealistic. In fact, it is quite pausible that relatively high NO mixing ratios

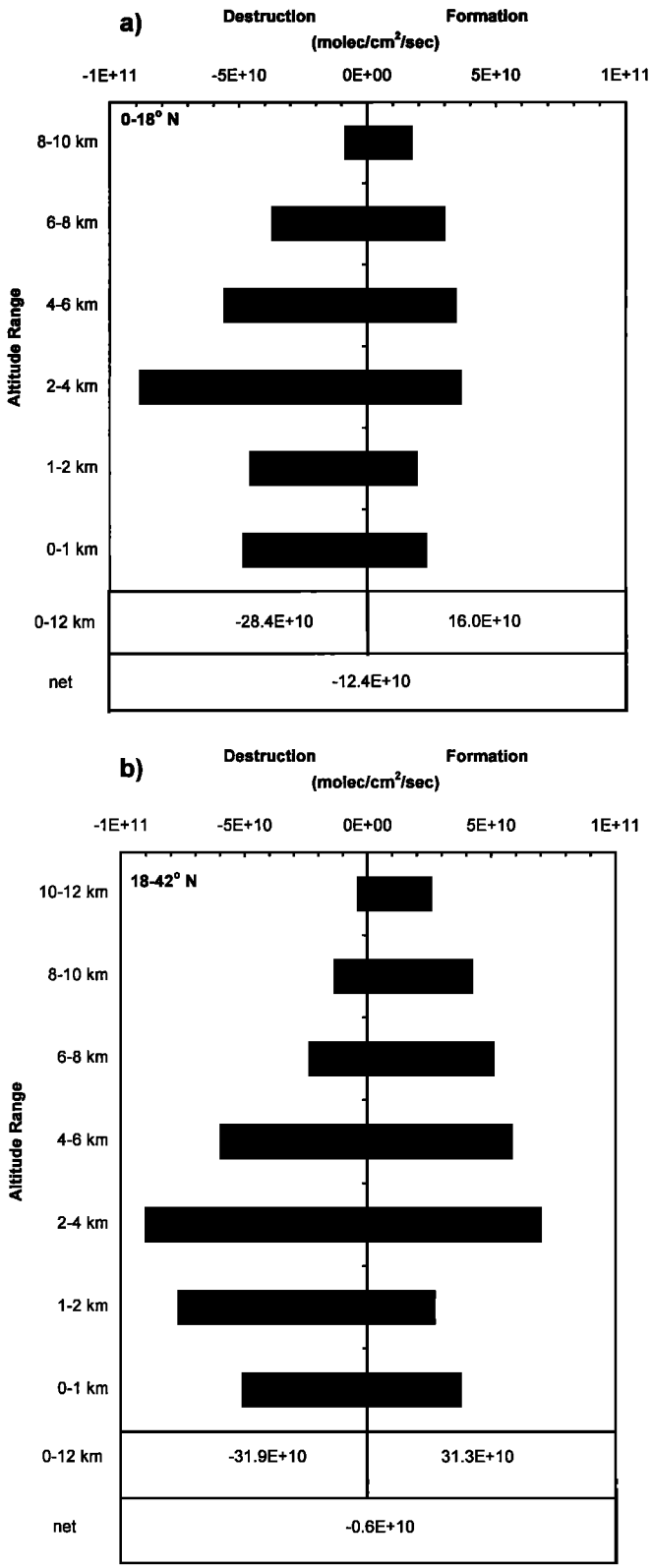

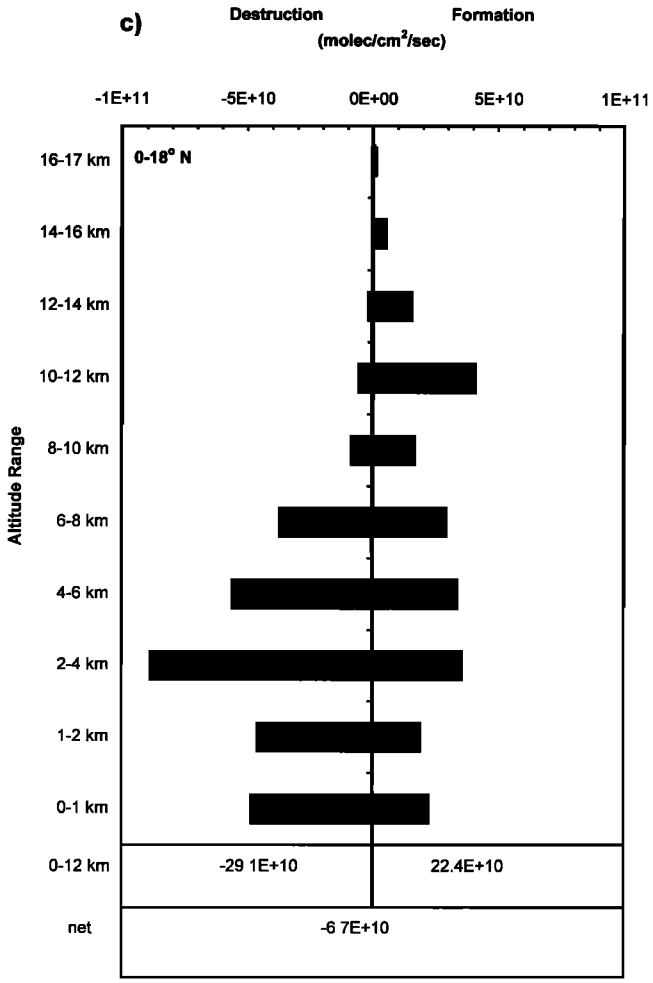

Figure 14. (continued)

Figure 14. Column-integrated diurnal-averaged $F(O_3)$ and $D(O_3)$ from TD modeling runs for the latitude ranges (a) 0°-18°N, 18°-42°N, and (c) 0°-18°N. Bars indicate contributions from each altitude bin to the total column. Formation and destruction column totals as well as the net impact of photochemistry on the total column O_3 are shown annotated at the bottom of each figure. Figure 14c indicates the effect of extending the O_3 column formation and destruction in the tropics from 10 km to the tropopause (see discussion in text).

above 10 km might be the result of lightning generated NO over tropical continental regions which, in turn, could be transported into the Pacific by large scale circulation such as the Walker circulation. At 150 pptv, the Δ increase in integrated column O_3 formation is $\sim 6 \times 10^{10}$ molecules/cm^2/s. If, in addition, 0.5 ppbv of acetone is added to this high-altitude mix, as reported by *H. Singh et al.* [manuscript in preparation, 1995], the tropical O_3 column deficit is reduced to $\sim 4 \times 10^{10}$ molecules/cm^2/s, or 13% of the total column destruction rate. This is well within the uncertainties of the calculations and may therefore represent a viable explanation. The fact that a deficit still remains, however, would seem to argue against there being yet another major O_3 destruction mechanism operating in the troposphere.

Recall that earlier in the text the possibility that tropospheric iodine might catalytically destroy O_3 was briefly discussed. Using the PEM-West A CH_3I data as one indicator of the marine iodine source strength, *Davis et al.* [this issue] have further explored the iodine-O_3 question in terms of three possible iodocarbon source scenarios. Based on a simple one-dimensional model that incorporated a first-order diffusion process to describe vertical transport, this analysis resulted in three different I_x ($I_x = I + IO + HOI + HI + 2I_2O_2 + INO_x$) altitudinal distributions. For the upper troposphere the I_x levels were 0.5, 1.5, and 7 pptv. Box modeling runs based on these I_x levels indicated that only at the 1.5 and 7 pptv level was there significant O_3 destruction.

Changes in total column-integrated O_3 destruction were $1.8x10^{10}$ and $9x10^{10}$ molecules/cm^2/s, respectively. The I_x value corresponding to the higher destruction was estimated based on a marine iodine source region having high biological productivity. However, during PEM-West A all sampling in the tropics occurred over low productivity marine water. Thus Davis et al. concluded that the impact of iodine on the column-integrated destruction of O_3 in the tropics was probably no greater than 6 %.

A comparison of O_3 budget estimates from this study with model estimates by *Fehsenfeld and Liu* [1993], shows reasonable agreement between the two studies. For example, using Fehsenfeld and Liu's altitude criteria for the free-troposphere, 1-12 km, we estimate an average column-integrated O_3 formation of $24x10^{10}$ molecules/cm^2/s. (In this evaluation an assumed value for $F(O_3)$ of $1x10^{10}$ molecules/cm^2/s was used for the altitude interval of 10-12 km in the tropics). When converted to similar units, Fehsenfeld and Liu's results would suggest an average value of $30x10^{10}$ molecules/cm^2/s, i.e., a factor of 1.25 times higher than this study. We note that these authors, with the exception of an observational altitude profile for the NO mixing ratio, based their results on generic global data.

Summary and Conclusions

When examined in terms of photochemical ozone processes, the PEM-West A data set was best described in terms of two geographical domains: the western North Pacific rim (WNPR) and the western tropical North Pacific (WTNP). The first region is one that was influenced by both natural and anthropogenic continental sources. High-altitude outflow from the Asian continent as well as from other northern hemispheric continents appear to have been involved. By contrast, the tropical regime, for altitudes less than 10 km, can be viewed as a region whose chemical fingerprint reflected either aged/well-processed continental air or air masses that had their origin in the tropical/equatorial Pacific.

In all cases the photochemical destruction of ozone, $D(O_3)$, was found to decrease more rapidly with altitude than photochemical formation, $F(O_3)$. Thus the ozone tendency, $P(O_3)$, typically was negative at low-altitudes (e.g., <6 km) but positive for altitudes >6 to 8 km. The most important chemical factor controlling the altitude trend in $D(O_3)$ was the H_2O mixing ratio. In most cases, (R4) was the dominant O_3 loss reaction, although at the highest altitudes the contribution from (R9) and (R10) increased significantly, with (R9) in some cases becoming dominant. The trend in $F(O_3)$ with altitude showed very modest decreases, reflecting the fact that decreases in HO_x radical levels with altitude were substantially offset by increases in the mixing ratio of NO. For altitudes <4 km the two most important ozone formation processes were identified as (R5) and (R6); whereas for altitudes >4 km (R5) was the dominant process (i.e., 55-85%). At all altitudes and all latitudes the contribution from (R7) was 11% or less. This observation indicates that NMHC emissions were typically of minor importance as ozone precursor species during the time period of PEM-West A.

A synoptic analysis of the PEM-West A database by several different investigating groups resulted in five different air mass classification schemes. These were examined here in terms of their respective values of $P(O_3)$. The general trend that emerged showed that the largest positive values occurred for BL air, within 2 days of mainland Asia or Japan and for high-altitude air parcels (e.g., >7 km) influenced by deep convection/lightning. Significant negative values of $P(O_3)$ were found when encountering clean marine BL air or relatively clean lower free-tropospheric air parcels.

When median values of the ratio NO_x/C_3H_8 were plotted against altitude or the ratio, C_2H_2/CO, the resulting profiles were found to be most consistent with the major sources of NO_x being located in the upper troposphere. Results generated by other PEM-West A investigators as well as further work by these authors suggest that one of the major contributors to this high-altitude NO_x pool was deep convection, especially that associated with lightning. Other contributing high-altitude primary NO_x sources appear to include aircraft emissions and stratospheric intrusions. Much more difficult to assess was the degree to which recycled NO_y contributed to the observed levels of NO_x. Potential uncertainties in measured NO_y and HNO_3 as well as possible incompleteness in the model chemistry represent the primary reasons for a lack of a more definitive statement on this important topic. In spite of these shortcomings, it still may be argued that the overall importance of recycled NO_x was higher in the western tropical Pacific than for the Pacific rim region.

Diurnal-averaged column-integrated photochemical formation and destruction fluxes for the WNPR region were shown to exceed those for NH dry deposition and NH stratospheric injection by factors of nearly 6. For this same region a near balance was found between photochemical O_3 production and destruction, suggesting that this region was near steady state. Ozone column lifetime arguments, together with small seasonal changes in total column O_3, suggest that the tropical regime should also have been near steady state. In fact, the column-integrated fluxes show that photochemical destruction exceeded production by nearly 80%. Two hypotheses were put forward in an effort to explain this deficit. The first involved the possibility that O_3-rich air could have been transported from midlatitudes into the tropics; the second proposed that the unsampled atmospheric column from 10 to 17 km might have provided the additionally needed photochemical O_3. The latter hypothesis requires relatively high levels of NO (e.g., 150 pptv); however, these do not appear to be totally out of line with those estimated from tropical lightning. In this context, results from the present study indicate that NO_x would have an extended lifetime at altitudes of 8-12 km of 3 to 9 days and even longer for still higher altitudes. This suggests that for some seasons of the year, deep convection over regions of Asia and Malaysia/Indonesia could lead to significant enhancements in high-altitude O_3 formation that might extend well out into the North Pacific. When coupled with very strong high-altitude westerly flow, its influence could potentially span a large part of the Pacific.

Acknowledgements. This work was supported in part by funds from the National Aeronautics and Space Administration under grants NCC-1-148 and 1438 and by the Atmospheric Chemistry Project of the Climate and Global Change Program of the National Oceanic and Atmospheric Administration. D. D. Davis would also like to thank the project office at NASA Langley Research Center and the flight crews at NASA Ames Research Center.

References

Barrie, L. A., J. W. Bottenheim, R. C. Shnell, P. J. Crutzen, and R. A. Rasmussen, Ozone destruction and photochemical reactions at polar sunrise in the lower Arctic atmosphere, *Nature, 334,* 138-141, 1988.

Blake, D. R., D. F. Hurst, T. W. Smith Jr., W. J. Whipple, T. -Y. Chen, N. J. Blake, and F. S. Rowland, Summertime measurements of selected nonmethane hydrocarbons in the Arctic and sub-arctic during the 1988 Arctic Boundary Layer Expedi tion (ABLE 3A), *J. Geophys. Res., 97,* 16,559-16,588, 1992.

Blake, D. R., T. W. Smith Jr., T. -Y. Chen, W. J. Whipple, and F. S. Rowland, Effects of biomass burning on summertime nonmethane hydrocarbons concentrations in the Canadian wetlands, *J. Geophys. Res., 99,* 1699-1719, 1994.

Blake, D. R., T.-Y. Chen, T. W. Smith Jr., C. J.-L. Wang, O. W. Wingenter, N. J. Blake, F. S. Rowland, and E. W. Mayer, Three dimensional distribution of NMHCs and halocarbons over the northwestern Pacific during the 1991 PEM West A, *J. Geophys. Res.,* this issue.

Bottenheim, J. W., L. A. Barrie, E. Atlas, L. E. Heidt, H. Niki, R. A. Rasmussen, and P. B. Shepson, Depletion of lower-tropospheric ozone during Arctic spring: The Polar Sunrise Experiment 1988, *J. Geophys. Res., 95,* 18,555-18,568, 1990.

Browell, E. V., et al., Large-scale air mass characteristics observed over the western Pacific during the summertime, *J. Geophys. Res.,* this issue.

Chameides, W. L., and J. C. G. Walker, A photochemical theory of tropospheric ozone, *J. Geophys. Res., 78,* 8751-8760, 1973.

Chameides, W. L., and D. D. Davis, Iodine: Its possible role in tropospheric photochemistry, *J. Geophys. Res., 85,* 7383-7398, 1980.

Chameides, W. L., and A. Tan, The two-dimensional diagnostic model for tropospheric OH: An uncertainty analysis, *J. Geophys. Res., 86,* 5209-5223, 1981.

Chameides, W., D. Davis, M. Rodgers, J. Bradshaw, S. Sandholm, G. Sachse, G. Hill, G. Gregory, and R. Rasmussen, Net ozone photochemical production over the eastern and central North Pacific as inferred from GTE/CITE 1 observations during fall 1983, *J. Geophys. Res., 92,* 2131-2152, 1987.

Chameides, W., D. Davis, G. Gregory, G. Sachse, and A. Torres, Ozone precursors and ozone photochemistry over eastern North Pacific Ocean during the Spring of 1984 based on the NASA GTE/CITE 1 airborne observations, *J. Geophys. Res., 94,* 9799-9808, 1989.

Chatfield, R. B., and P. J. Crutzen, Are there interactions of iodine and sulfur species in marine air photochemistry?, *J. Geophys. Res., 95,* 22,319-22,341, 1990.

Chatfield, R. and A. Delany, Convection links biomass burning to increased tropical ozone: However, models will tend to overpredict O_3, *J. Geophys. Res., 95,* 18,473-18,488, 1990.

Chatfield, R., and H. Harrison, Ozone in the remote troposphere: Mixing versus photochemistry, *J. Geophys. Res., 81,* 421-423, 1976.

Crawford, J., et al., A photostationary state analysis of the NO_2-NO system based on airborne observations from the western and central North Pacific, *J. Geophys. Res.*, this issue.

Crosley, D. R., NO_y Blue Ribbon panel, *J. Geophys. Res.*, this issue.

Crutzen, P., A discussion of the chemistry of some minor constitu ents in the stratosphere and troposphere, *Pure Appl. Geophys., 106-108,* 1385-1399, 1973.

Davis, D. D., et al., A photostationary state analysis of the NO_2-NO system based on airborne observations from the subtropical/tropical North and South Atlantic, *J. Geophys. Res., 98,* 23,501-23,523, 1993.

Davis, D., J. Crawford, S. Liu, S. McKeen, A. Bandy, D. Thornton, F. Rowland, and D. Blake, Potential impact of iodine on tropospheric levels of ozone and other critical oxidants, *J. Geophys. Res.*, this issue.

Fabian, P., Comments on 'A photochemical theory of tropospheric ozone' by W. Chameides and J. C. G. Walker, *J. Geophys. Res., 79,* 4124-4125, 1974.

Fabian P., and P. G. Pruchniewicz, Meridional distribution of ozone in the troposphere and its seasonal variation, *J. Geophys. Res., 82,* 2063-2073, 1977.

Fan, S.-M., D. J. Jacob, D. L. Mauzerall, J. D. Bradshaw, S. T. Sandholm, D. R. Blake, H. B. Singh, R. W. Talbot, G. L. Gregory, and G. W. Sachse, Origin of tropospheric NO_x over subarctic eastern Canada in summer, *J. Geophys. Res., 99,* 16,867-16,877, 1994.

Fehsenfeld, F., and S. Liu, Tropospheric ozone: Distribution and sources in, *Global Atmospheric Chemical Change,* edited by C. Hewitt and W. Sturges, Elsevier Science, New York, pp. 169-231, 1993.

Fishman, J., and P. Crutzen, The origin of ozone in the tropo sphere, *Nature, 274,* 855-858, 1978.

Fishman, J., S. Solomon, and P. Crutzen, Observational and theoretical evidence in support of a significant in-situ photochemical source of tropospheric ozone, *Tellus, 31,* 432-446, 1979.

Fishman, J., C. Watson, and J. Larsen, and J. Logan, Distribution of tropospheric ozone determined from satellite data, *J. Geophys. Res., 95,* 3599-3617, 1990.

Gidel, L. T., and M. A. Shapiro, General circulation model estimates of the net vertical flux of ozone in the lower stratosphere and the implications for the tropospheric ozone budget, *J. Geophys. Res., 85,* 4049-4058, 1980.

Gregory, G. L., A. S. Bachmeier, D. R. Blake, B. G. Heikes, D. C. Thornton, J. D. Bradshaw, and Y. Kondo, Chemical signature of aged Pacific marine air: Mixed layer and free-troposphere as measured during PEM West A, *J. Geophys. Res.*, this issue.

Heikes, B. G., et al., Hydrogen peroxide and methylhydroperoxide distributions related to ozone and odd-hydrogen over the north Pacific in the Fall of 1991, *J. Geophys. Res.*, this issue.

Hoell, J. M., D. D. Davis, S. C. Liu, R. Newell, M. Shipham, H. Akimoto, R. J. McNeal, R. J. Bendura, and J. W. Drewry, Pacific Exploratory Mission-West (PEM-West A): September-October 1991, *J. Geophys. Res.*, this issue.

Jacob, D., et al., Summertime photochemistry of the troposphere at high northern latitudes, *J. Geophys. Res., 97,* 16,421-16,431, 1992.

Jenkin, M. E., A comparative assessment of the role of iodine photochemistry in tropospheric ozone depletion, in *The Tropo spheric Chemistry of Ozone in the Polar Regions,* edited by H. Niki and K. H. Becker, Springer-Verlag, New York, 1993.

Jobson, B. T., H. Niki, Y. Yokouchi, J. Bottenheim, F. Hopper, and R. Leaitch, Measurements of C_2-C_6 hydrocarbons during Polar Sunrise 1992 Experiment: Evidence for Cl atom and Br atom chemistry, *J. Geophys. Res., 99,* 25,355-25,368, 1994.

Johnson, J. E., R. H. Gammon, J. Larsen, T. S. Bates, S. J. Oltmans, and J. C. Farmer, Ozone in the marine boundary layer over the Pacific and Indian oceans: Latitudinal gradients and diurnal cycles, *J. Geophys. Res., 95,* 11,847-11,856, 1990.

Kawa, S. R., and R. Pearson Jr., Ozone budgets from the dynamics and chemistry of marine stratocumulus experiment, *J. Geophys. Res., 94,* 9809-9817, 1989.

Keene, W. C., A. A. P. Pszenny, D. J. Jacob, R. A. Duce, J. N. Galloway, J. J. Schultz-Tokos, H. Sievering, and J. F. Boatman, The geochemical cycling of reactive chlorine through the marine troposphere, *Global Biogeochem. Cycles, 4,* 407-430, 1990.

Kondo, Y., H. Ziereis, M. Koike, S. Kawakami, G. L. Gregory, G. W. Sachse, J. B. Singh, D. D. Davis, and J. T. Merrill, Reactive nitrogen over the Pacific Ocean during PEM-West A, *J. Geophys. Res*, this issue.

LeBras, G., and U. Platt, A possible mechanism for combined chlorine and bromine catalyzed destruction of tropospheric ozone in the Arctic, *Geophys. Res. Lett., 22,* 599-602, 1995.

Lenschow, D. H., R. Pearson Jr., and B. B. Stankor, Measure ments of ozone vertical flux to ocean and forest, *J. Geophys. Res., 87,* 8833-8837, 1982.

Liu, S. C., D. Kley, M. McFarland, J. D. Mahlman, and H. Levy II, On the origin of tropospheric ozone, *J. Geophys. Res., 85,* 7546-7552, 1980.

Liu, S. C., M. McFarland, D. Kley, O. Zafiriou, and B. Huebert, Tropospheric NO_x and O_3 budgets in the equatorial Pacific, *J. Geophys. Res., 88,* 1360-1368, 1983.

Liu, S. C., M. Trainer, F. C. Fehsenfeld, D. D. Parrish, E. J. Williams, D. W. Fahey, G. Hubler, and P. C. Murphy, Ozone production in the rural troposphere and the implications for regional and global ozone distributions, *J. Geophys. Res.*, *92*, 4191-4207, 1987.

Liu, S. C., et al., A study of the photochemistry and ozone budget during the Mauna Loa Observatory Photochemistry Experiment, *J. Geophys. Res.*, *97*, 10,463-10,471, 1992.

Liu, S. C., et al., A model study of tropospheric trace species distribution during PEM-West A, *J. Geophys. Res.*, this issue.

Logan, J. A., M. J. Prather, S. C. Wofsy, and M. B. McElroy, Tropospheric chemistry: A global perspective, *J. Geophys. Res.*, *86*, 7210-7254, 1981.

Luke, W. T., R. R. Dickerson, W. F. Ryan, K. E. Pickering, and L. J. Nunnermacker, Tropospheric chemistry over the lower Great Plains of the United States 2. Trace gas profiles and distributions, *J. Geophys. Res.*, *97*, 20,647-20,670, 1992.

Mahlman, J. D., H. Levy II, and W. J. Moxim, Three-dimen sional tracer structure and behavior as simulated in two ozone precursor experiments, *J. Atmos. Sci.*, *37*, 655-685, 1980.

McFarland, M., D. Kley, J. W. Drummond, A. L. Schmeltekopf, and R. H. Winkler, Nitric oxide measurements in the equatorial Pacific region, *Geophys. Res. Lett.*, *6*, 605-608, 1979.

McKeen, S. A., E. Y. Hsie, M. Trainer, R. Tallmraju, and S. C. Liu, A regional model study of the ozone budget in the eastern United States, *J. Geophys, Res.*, *96*, 10,809-10,845, 1991.

Merrill, J. T., Trajectory results and interpretation for PEM-West A, *J. Geophys. Res.*, this issue.

Pickering, K. E., A. M. Thompson, R. R. Dickerson, W. T. Luke, D. P. McNamara, J. P. Greenberg, and P. R. Zimmerman, Model calculations of tropospheric ozone production potential following observed convective events, *J. Geophys. Res.*, *95*, 14,049-14,062, 1990.

Pickering, K. E., A. M. Thompson, W.-K. Tao, and T. L. Kucsera, Upper tropospheric ozone production following mesoscale convection during STEP/EMEX, *J. Geophys. Res.*, *98*, 8737-8749, 1993.

Piotrowicz, S. R., D. A. Boran, and C. K. Fischer, Ozone in the boundary layer of the equatorial Pacific Ocean, *J. Geophys. Res.*, *91*, 13,113-13,119, 1986.

Ridley, B. A., M. A. Carroll, and G. L. Gregory, Measurements of nitric oxide in the boundary layer and free-troposphere over the Pacific Ocean, *J. Geophys. Res.*, *92*, 2025-2047, 1987.

Singh, H. B., and J. F. Kasting, Chlorine-hydrocarbon photochem istry in the marine troposphere and lower stratosphere, *J. Atmos. Chem.*, *7*, 261-285, 1988.

Singh, H. B., D. O'Hara, D. Herlth, J. D. Bradshaw, S. T. Sandholm, G. L. Gregory, G. W. Sachse, D. R. Blake, P. J. Crutzen, and M. A. Kanakidou, Atmospheric measurements of peroxyacetyl nitrate and other organic nitrates at high latitudes: Possible sources and sinks, *J. Geophys. Res.*, *97*, 16,511-16,522, 1992.

Singh, H. B., et al., Summertime distribution of PAN and other reactive nitrogen species in the northern high-latitude atmosphere of eastern Canada, *J. Geophys. Res.*, *99*, 1821-1835, 1994.

Singh, H. B., et al., Low ozone in the marine boundary layer of the tropical Pacific Ocean: Photochemical loss, chlorine atoms, and entrainments, *J. Geophys. Res.*, this issue.

Singh, H. B., et al., Reactive nitrogen and ozone over the western Pacific: Distribution, partitioning, and sources, *J. Geophys. Res.*, this issue.

Smyth, S., et al., Comparison of free-tropospheric western Pacific air mass classification schemes for the PEM-West A experiment, *J. Geophys. Res.*, this issue.

Solomon, S., R. R. Garcia, and A. R. Ravishankara, On the role of iodine in ozone depletion, *J. Geophys. Res.*, *99*, 20,491-20,499, 1995.

Talbot, R. W., et al., Chemical characteristics of continental outflow from Asia to the troposphere over the western Pacific Ocean during September-October, 1991 *J. Geophys. Res.*, this issue.

Thompson, A. M., and D. H. Lenschow, Mean profiles of reactive trace gases in the unpolluted marine surface layer, *J. Geophys. Res.*, *89*, 4788-4796, 1984.

Thompson A. M., et al., Ozone observations and a model of marine boundary layer photochemistry during SAGA 3, *J. Geophys. Res.*, *98*, 16,955-16,968, 1993.

Wayne, R. P., et al., The nitrate radical: Physics, chemistry, and the atmosphere, *Atmos. Environ.*, *25A*, 1-203, 1991.

B. Anderson, A. Bachmeier, J. Barrick, E. Browell, J. Collins, G. Gregory, and G. Sachse, NASA Langley Research Center, Hampton, Virginia 23681.

D. Blake and S. Rowland, Chemistry Department, University of California-Irvine, Irvine, California 92717.

J. Bradshaw, W. Chameides, G. Chen, J. Crawford, D. D. Davis (corresponding author), and Scott Sandholm, School of Earth and Atmospheric Sciences, Georgia Institute of Technology, Atlanta, Georgia 30332.

B. Heikes and J. Merrill, Graduate School of Oceanography, University of Rhode Island, South Ferry Road, Narragansett, Rhode Island 02882-1197

Y. Kondo, Solar Terrestrial Environmental Lab, Nagoya University, Toyokawa, Aichi, Japan 442.

S. Liu, Environmental Research Labs, NOAA Aeronomy Laboratory R/E/AL-4, 325 Broadway, Boulder, Colorado 80303.

R. E. Newell, Massachusetts Institute of Technology, Depart-ment of Earth, Atmospheric and Planetary Sciences, Building 54, Cambridge, Massachusetts 02139.

J. Rodriguez, AER Incorporated, 840 Memorial Drive, Cambridge, Massachusetts 02139.

H. Singh, NASA Ames Research Center, Moffett Field, California 94035.

R. Talbot, Institute for the Study of Earth, Oceans, and Space, University of New Hampshire, 292 College Road, Durham, New Hampshire 03824.

(Received April 14, 1995; revised September 5, 1995; accepted September 5, 1995.)